Non-pumping reactive wells filled with mixing nano and micro zero-valent iron for nitrate removal from groundwater: Vertical, horizontal, and slanted wells

Politecnico di Torino

Non-Pumping Reactive Wells Filled with Mixing Nano and Micro Zero-Valent Iron for Nitrate Removal from Groundwater: Vertical, Horizontal, and Slanted Wells

Seiyed Mossa Hosseini[a] , Tiziana Tosco[b], Behzad Ataie-Ashtiani[c, d], Craig T. Simmons[e]

[a] Physical Geography Department, University of Tehran, P.O. Box 14155-6465, Tehran, Iran.

[b] Dipartimento di Ingegneria dell'Ambiente, del Territorio e delle Infrastrutture, Politecnico di Torino,Torino, Italy.

[c] Sharif University of Technology, P.O. Box 11155-9313, Tehran, Iran

[d] National Centre for Groundwater Research & Training and School of the Environment, Flinders University, GPO Box 2100, Adelaide, South Australia 5001, Australia.

[e] National Centre for Groundwater Research & Training and School of the Environment, Flinders University, GPO Box 2100, Adelaide, South Australia 5001, Australia.

Corresponding Author: Seiyed Mossa Hosseini, smhosseini@ut.ac.ir (S.M. Hosseini).

Original Citation:

S. M. Hosseini, T. Tosco, B. Ataie-Ashtiani, C. G. Simmons (2018), A Non-Pumping Reactive Wells Filled with Mixing Nano and Micro Zero-Valent Iron for Nitrate Removal from Groundwater: Vertical, Horizontal, and Slanted Wells. Journal of Contaminant Hydrology 210, pp. 50-64. - ISSN 0169-7722

Non-Pumping Reactive Wells Filled with Mixing Nano and Micro Zero-Valent Iron for Nitrate Removal from Groundwater: Vertical, Horizontal, and Slanted Wells

Seiyed Mossa Hosseini[a,1], Tiziana Tosco[b], Behzad Ataie-Ashtiani[c, d], Craig T. Simmons[e]

[a] Physical Geography Department, University of Tehran, P.O. Box 14155-6465, Tehran, Iran.

[b] Dipartimento di Ingegneria dell'Ambiente, del Territorio e delle Infrastrutture, Politecnico di Torino,Torino, Italy.

[c] Sharif University of Technology, P.O. Box 11155-9313, Tehran, Iran

[d] National Centre for Groundwater Research & Training and School of the Environment, Flinders University, GPO Box 2100, Adelaide, South Australia 5001, Australia.

[e] National Centre for Groundwater Research & Training and School of the Environment, Flinders University, GPO Box 2100, Adelaide, South Australia 5001, Australia.

Abstract

Non-pumping reactive wells (NPRWs) filled by zero-valent iron (ZVI) can be utilized for the remediation of groundwater contamination of deep aquifers. The efficiency of NPRWs mainly depends on the hydraulic contact time (HCT) of the pollutant with the reactive materials, the extent of the well capture zone (W_{cz}), and the relative hydraulic conductivity of aquifer and reactive material (K_r). We investigated nitrate removal from groundwater using NPRWs filled by ZVI (in nano and micro scales) and examined the effect of NPRWs orientations (i.e. vertical, slanted, and horizontal) on HCT and W_{cz}. The dependence of HCT on W_{cz} for different K_r values was derived theoretically for a homogeneous and isotropic aquifer, and verified using particle tracking simulations performed using the semi-analytical particle tracking and pathlines model (PMPATH). Nine batch experiments were then performed to investigate the impact of mixed nano-ZVI, NZVI (0 to 2 $g\ l^{-1}$) and micro-ZVI, MZVI (0 to 4 $g\ l^{-1}$) on the nitrate removal rate (with initial NO_3^-=132 $mg\ l^{-1}$). The NPRWs system was tested in a bench-scale sand medium (60 cm length × 40 cm width × 25 cm

[1] Corresponding Author. *Email address*: smhosseini@ut.ac.ir (S.M. Hosseini).

height) for three orientations of NPRWs (vertical, horizontal, and slanted with inclination angle of 45°). A mixture of nano/micro ZVI, was used, applying constant conditions of pore water velocity (0.024 $mm\ s^{-1}$) and initial nitrate concentration (128 $mg\ l^{-1}$) for five pore volumes. The results of the batch tests showed that mixing nano and micro Fe^0 outperforms these individual materials in nitrate removal rates. The final products of nitrate degradation in both batch and bench-scale experiments were NO_2^-, NH_4^+, and $N_2(gas)$. The results of sand-box experiments indicated that the slanted NPRWs have a higher nitrate reduction rate (57%) in comparison with vertical (38%) and horizontal (41%) configurations. The results also demonstrated that three factors have pivotal roles in expected HCT and W_{cz}, namely the contrast between the hydraulic conductivity of aquifer and reactive materials within the wells, the mass of Fe^0 in the NPRWs, and the orientation of NPRWs adopted. A trade-off between these factors should be considered to increase the efficiency of remediation using the NPRWs system.

Key-Words: Non-Pumping Reactive Wells; nitrate Reduction; Groundwater contamination; Remediation; Nano and Micro Zero-valent Iron; Slanted Well; Capture Zone of Well.

1. Introduction

Nitrate is a universal, ubiquitous groundwater pollutant that constitutes a major health risk to humans and a burden on the environment (Gandhi et al., 2002). This widespread contaminant leaches into the groundwater from anthropogenic sources (e.g. nitrogen fertilizers, animal waste, and septic systems), irrigation and runoff from farmlands. Among common denitrification technologies (i.e. biological and chemical reduction) (Rocca et al., 2007), the abiotic chemical reduction of nitrate by zero-valent iron (ZVI) has been effectively implemented (Ludwig and Jekel, 2007). Chemical reduction of NO_3^- by nano-scale ZVI (NZVI) has gained its application since 1990s (Tratnyek et al., 2003; Grieger et al., 2010), although NO_3^- reduction by Fe^0 was reported earlier by Young et al. (1964). One of the well-known approaches for in-situ nitrate treatment in groundwater is emplacing the ZVI particles in permeable reactive barriers (PRBs), with different configurations, namely continuous trenches, funnel-and-gate or reactive vessel (Day et al., 1999; Hosseini et al., 2011a). These configurations are typically limited to groundwater depths less than approximately 20 m (U.S. Environmental Protection Agency, USEPA, 1998), and consequently cannot be utilized for the remediation of deep groundwater contamination (Freethey et al., 2002). Arrays of non-pumping reactive wells (NPRWs) have been studied as an appropriate alternative for application to deeper aquifer systems (Wilson et al., 1997, Hosseini and Tosco, 2015).

The construction of NPRWs arrays is a promising and cost-effective alternative emplacement method for contamination plumes deeper than 50 m (Wilson and Mackay, 1997; Puls et al., 1999; Wilkin et al., 2002). The efficiency of NPRWs filled by ZVI in treating a groundwater contaminated plume is controlled by several key aspects, including aquifer hydrology (e.g. flow velocity, prevalent flow direction, hydraulic conductivity, porosity, depth and fluctuations of water table, and heterogeneity), groundwater geochemistry (e.g. concentration of pollutants, geometry and depth of contaminated plume, pH, dissolved oxygen, type and

concentration of dissolved salts), configuration of NPRWs (e.g. diameter and length of wells, space between wells, design of screen), characteristics of the reactive material (e.g. particle size, Fe^0 content, eventual surface modifier), contact time (or residence time) needed for the reaction between contaminant and reactive agents, and difference in hydraulic conductivity between the reactive material and the aquifer medium (Wilson et al., 1997; Freethey et al., 2002; Painter, 2004; Hosseini et al., 2011b; Hosseini and Tosco, 2013).

The installation of horizontal and slanted wells has become popular since the 1930s, in the petroleum industry, and recently for the recovery of contaminated groundwater, collecting non-aqueous phase liquids and soil vapor from the subsurface, drainage, and mine dewatering (Hantush and Papadopulos, 1962; Tsou et al., 2010). Bearing in mind the higher cost of drilling horizontal wells, they have some advantages over vertical wells: their geometry improves the contact with contaminated groundwater, and they are suitable to install in thin aquifers (Zhan and Zlotnik, 2002); horizontal and slanted wells produce less pronounced drawdown cones, and are more suitable for groundwater flow with significant vertical velocity component and pronounced fluctuations of the water table (Morgan, 1992; Kompani-Zare et al., 2005; Huang et al., 2011); drilling operations of horizontal and slanted wells are a more doable option when surface structures (e.g. buildings) are present at the surface. Furthermore, due to the significant advances of the directional drilling technology over the last two decades and the cost reduction in their installation procedures (Liang et al., 2016), interest in the application of horizontal and slant pumping wells has been reignited. To date, the horizontal and slant pumping wells are commonly installed in shallow aquifers to withdraw a large amount of groundwater (Bear, 1979) or to remove a large amount of contaminant (Sawyer and Lieuallen-Dulam, 1998). Readers are encouraged to refer to Yeh and Chang (2013) for a recent and comprehensive review of groundwater flow hydraulics modelling of the horizontal and slant pumping wells. To the best of our knowledge, in spite of

the aforementioned advantages of slanted or horizontal wells, no previous work could be found that investigates the efficiency of these wells for the emplacement of the reactive materials for groundwater remediation.

There are a very limited number of studies that investigate the efficiency of vertical NPRWs as reactive barriers. High removal rate of chromate from contaminated groundwater at North Carolina (Puls et al., 1999) and chlorinated hydrocarbon compounds at Denver Federal Center, Colorado (Wilkin et al., 2002) are reported for iron-filled NPRWs arrays. Mixtures of bone-char phosphate and iron oxide were deployed in arrays of NPRWs at two sites: Christensen Ranch In-Situ U Mine, Wyoming and Fry Canyon, Utah (Naftz et al., 2002). Initial U removal efficiencies exceeded 99.9% during a 7-month deployment period at the Christensen Ranch site. In a previous study, Hosseini and Tosco (2015) reported a successful application of biochemical remediation of a nitrate contaminated bench-scale aquifer by emplacing a combination of NZVI and carbon substrates in an array of vertical NPRWs.

The motivation of this study is to answer these questions: are the aforementioned advantages of horizontal and slanted pumping wells also extendable when these wells serve as non-pumping reactive wells to remediate nitrate contaminated groundwater? Precisely, how would the progress of the denitrification process through NPRWs be influenced by different well orientations in the presence of nano and micro Fe^0 particles as reactive materials?

To answer these questions and to gain an understanding on the applicability of slanted NPRWs systems, connection between hydraulic parameters of aquifer, chemical reduction of NO_3^- by mixing NZVI and MZVI, and orientation of NPRWs should be analyzed. In this study, nitrate removal process was investigated in vertical, horizontal, and slant NPRWs filled by mixing nano/micro ZVI positioned in a homogeneous and isotropic bench-scale sand medium. Batch experiments were also performed to investigate the effect of mass of ZVI particles, type of reagents (i.e. micro or nano or a mixture of both) on the denitrification

process under constant initial nitrate concentration. The main focus of bench-scale experiments was to modify the contact time of nitrate and reactive materials by changing NPRWs orientation, whereas other factors (e.g. initial nitrate concentration, mass of Fe^0, pore water velocity) were considered constant.

This paper is organized as follows (Fig. 1): we first consider the hydrodynamic aspects related to the NPRWs, presenting analytical equations for computing the hydraulic contact time and capture area for a NPRW in three orientations (vertical, horizontal, and slanted with inclination angle of 45°) (section 2.1 and 3.1). Homogeneous and isotropic aquifer and steady-state flow condition were assumed. The effect of relative hydraulic conductivity between aquifer material and reactive media is then investigated. Batch experiments were established to investigate the effect of mixing two reagents NZVI (0-8 $g\ l^{-1}$) and MZVI (0-16 $g\ l^{-1}$) on the nitrate reduction and nitrogen byproducts (section 2.2 and 3.2). Kinetic analysis of nitrate reduction and ammonium stripping and production were also conducted based on batch experiments (section 2.4.). The best mixing ratio of micro and nano ZVI for nitrate reduction obtained in batch experiments was selected to implement NPRWs systems with vertical, horizontal, and slanted orientations of wells at a bench-scale (section 2.3 and 3.3).

2. Material and Methods

2.1. Hydraulic Contact Time and Area of Well Capture Zone Computations

Assuming a homogenous and isotropic aquifer with hydraulic conductivity K_{aq} and horizontal flow, where a vertical NPRW filled with a reactive material having an hydraulic conductivity K_{rm}, the hydraulic contact time, HCT (or residence time) between the contaminant and reactive agents can be obtained using Darcy law and continuity principle. Figure 2 shows the capture area for a vertical NPRW at steady state flow condition, for a

given hydraulic contrast K_{rm}/K_{aq} =80, simulated by particle tracking and pathlines model, PMPATH. The streamlines passing through the center and borders of NPRW have the longest (L_{max}) ad shortest (L_{min}) flow path. The discharge through the upgradient capture zone of the NPRW (Q_{cz} $[L^3T^{-1}]$) must pass through the reactive materials (Q_{rm} $[L^3T^{-1}]$), thus:

$$Q_{cz} = Q_{rm} \quad (1)$$

According to Darcy law and variables defined in Fig. 2, the Eq. 1 can be written as

$$K_{aq} \times i_{aq} \times W_{cz} \times L_w = K_{rm} \times i_{rm} \times D_w \times L_w \quad (2)$$

where $i_{aq}[-]$ and $i_{rm}[-]$ are the hydraulic gradient of aquifer and reactive materials, respectively; $D_w[L]$ is well diameter, $L_w[L]$ is length of well, and $W_{cz}[L]$ is the width of capture zone, as shown in Fig. 2. Replacing the $K_{aq} \times i_{aq}$ by $V_{aq} \times n_{aq}$ (where V_{aq} and n_{aq} are pore water velocity and porosity), the Eq. 2 become as

$$V_{aq} \times n_{aq} \times W_{cz} = K_{rm} \times i_{rm} \times D_w \quad (3)$$

or

$$i_{rm} = \frac{V_{aq} \times n_{aq} \times W_{cz}}{K_{rm} \times D_w} \quad (4)$$

This expression can be used in the computation of HCT. Considering the median flow path through the NPRW, L_{med} $[L]$, the average contact time between the contaminant plume and reactive agents, t_c $[T]$ is

$$t_c = \frac{L_{med}}{V_{rm}} = \frac{L_{med} \times n_{rm}}{K_{rm} \times i_{rm}} \quad (5)$$

Substituting the i_{rm} from Eq. 4

$$t_c = \frac{L_{med} \times n_{rm} \times D_w}{V_{aq} \times n_{aq} \times W_{cz}} = \frac{L_{med} \times D_w}{V_{aq} \times W_{cz}} \times n_R \quad (6)$$

where n_R $[-]$ is relative porosity (i.e. $n_R = n_{rm}/n_{aq}$). The area of capture zone, $a_{cz}[L^2]$ defined as the area perpendicular to the upgradient flow that the streamlines within this area pass through the NPRW (as shown in Fig. 2):

$$a_{cz} = W_{cz} \times L_w \tag{7}$$

Factor $f[-]$ is defined as the proportion of width of capture zone W_{cz} to the well diameter D_w. Replacing $f \times D_w$ for W_{cz} in the Eq. 2, following definition is obtained for the factor f:

$$f = \frac{K_{rm} \times i_{rm}}{K_{aq} \times i_{aq}} = K_R \times i_R = V_R \times n_R \tag{8}$$

where $i_R[-]$, $K_R[-]$, $V_R[-]$, and $n_R[-]$ are relative porosity ($i_R = i_{rm}/i_{aq}$), relative hydraulic conductivity ($K_R = K_{rm}/K_{aq}$), relative pore water velocity ($V_R = V_{rm}/V_{aq}$), and relative porosity ($n_R = n_{rm}/n_{aq}$), respectively.

Wheatcraft and Winterberg (1985) suggested the following expression for calculating the factor f in a uniform flow system around a vertical permeable cylinder:

$$f = \frac{2 \times K_R}{1 + K_R} \tag{9}$$

While the Eq. 9 obtains factor f as a function of K_R, the Eq. 8 incorporates the hydraulic gradient in the aquifer and in the reactive materials (as parameter i_R) beside K_R.

Combining the two Eqs. 6 and 8 the HCT of a contaminant plume intercepted by the a vertical NPRW can be computed as

$$t_c = \frac{L_{med} \times n_R}{V_{aq} \times K_R \times i_R} \tag{10}$$

Equation 10 can be extended for any orientation of NPRW with inclination angle $\hat{\theta}$ by dividing the right-hand-side (RHS) of Eq. 10 by $\cos\hat{\theta}$ (for vertical well $\hat{\theta}$=0). The t_c for the horizontal NPRW ($\hat{\theta}$=90°) can be obtained by multiplying the RHS of Eq. 10 in L_w/L_{med}.

The area of the capture zone $a_{cz}\,[L^2]$ for a horizontal NPRW ($\hat{\theta} = 90^\circ$) is a circle with diameter $W_{cz} = f \times D$. Whereas the a_{cz} for a fully-penetrating vertical NPRW ($\hat{\theta} = 0$) is

rectangular with dimensions of $W_{cz} \times L_w$ (see also Eq. 7). For a slanted NPRW with inclination angle $\hat{\theta}\epsilon(0,90)$, a_{cz} can be defined as:

$$a_{CZ} = W_{cz} \times L_{cz} \times \cos\hat{\theta} \tag{11}$$

where $L_{cz}[L]$ is the upgradient length of well capture zone, $L_{cz} = f \times L_w$. Using the expression above, the area of NPRW capture zone, a_{CZ}, can be written as

$$a_{CZ} = \begin{cases} \frac{\pi}{4} \times f^2 \times {D_w}^2 & for \quad \hat{\theta} = 90^{\circ} \\ f \times D_w \times L_w & for \ \hat{\theta} = 0 \\ f^2 \times D_w \times L_w \times \cos\hat{\theta} & for \ 0 < \hat{\theta} < 90^{\circ} \end{cases} \tag{12}$$

Figure 3 (a-c) indicates schematically the parameters a_{CZ}, W_{cz}, and L_{cz} for vertical, horizontal, and slanted NPRW.

2.2. Batch Experiments

To investigate the effects of the ratio of Fe^0/N on NO_3^- reduction by micro, nano, and mixing micro and nano Fe^0, batch experiments were conducted. The NZVI particles (NANOFER STAR, NANOIRON, Czech Republic) have a Fe^0 content of 90%, are stabilized by a thin layer of iron oxide, and have an average diameter of 50 nm, specific surface area of 20–25 m^2/g as reported by the manufacturer (see also http://nanoiron.cz). Aqueous solutions with initial NO_3^- concentration of 131±2 $mg\ l^{-1}$ were prepared by dissolving desired amount of KNO_3 in tap water. 250 ml of the prepared aqueous NO_3^- solution was put in nine glass beakers. Nine treatments (named A to I) containing different mass of micro and nano ZVI were considered to investigate the effect of each micro and nano particles dose individually, and of the mixing ratio on the nitrate removal rate. Table (1) provides the concentration of NZVI and MZVI used in the nine treatments. The Fe/NO_3^- mass ratios were also calculated and listed in Table (1). The batch experiments were continuously operated for 1200 h (50 days) to investigate the fate of denitrification processes in reducing/producing nitrogen

species. Shaking the beakers were conducted continuously in a slow-speed stirrer from the beginning of the experiment up to 160 h, and then they were kept in ambient conditions with one hour shaking per day, in order to obtain as much as possible a homogeneous mixing of reagent and solution. The head space was filled with Ar gas. Samples of 10 ml each were collected with a syringe at fixed times (up to 160 h after adding the particles) and then filtered by a 0.2 μm filter paper just before analysis by photometer for measuring the absorbance values of the sample. Immediately after the analysis of each sample, the corresponding headspace was filled by aqueous solution with the same concentration of nitrate of the extracted solution and the residue mass of Fe on filter paper is also added to the solution to keep constant the ration of ZVI/nitrate ratio throughout reaction time. The collected samples were passed through a 0.5 μm membrane filter, and analyzed for NO_3^-, NO_2^-, NH_4^+, EC, TDS, and pH. NO_3^-, NO_2^-, and NH_4^+ were measured by standard methods using a multi-parameters photometer (HI 83300, USA). The EC and pH variation in the solutions were also monitored using EC and resistivity portable meter (HI 87314, USA), and pH portable meter (HI 99151, USA), respectively. All analyses were conducted in duplicate to check the reproducibility of the experimental data. Experiments were conducted at ambient temperature (25 ± 2 °C).

2.3. Bench Scale Experimental Setup

The bench-scale laboratory setup was fabricated in Plexiglas, with dimensions of 60 cm (length) × 40 cm (width) × 25 cm (height) as shown schematically in Fig. 4. The box was packed with homogeneous, uncontaminated coarse sand (from Iranian Silica Sand MFG Company) with measured bulk density ρ_b=1.57 $g\ cm^{-3}$, grain size density ρ_s=2.67 $g\ cm^{-3}$, d_{50}=0.795 mm, hydraulic conductivity K_{aq} = 0.82 $mm\ s^{-1}$ (70.8 $m\ d^{-1}$), porosity n_{aq} = 0.41, and longitudinal dispersivity α_L= 4.05 mm.

Two screens were inserted at the inlet and outlet to establish a uniform flow through the soil (Fig. 4). The water level in the outlet reservoir was kept at the same level as the top of the sand in order to maintain saturated conditions through the experiments. A peristaltic pump (B-V Series, Etatron D.S., Italy) was used to feed the contaminated water at constant rate of 0.30 $l\,min^{-1}$ (i.e. pore water velocity V_{aq} = 0.025± 0.02 $mm\,s^{-1}$, and hydraulic gradient i_{aq}=0.012± 0.01) into the upstream reservoir through all experiments (Fig. 4). An average travel time through sand medium (i.e. pore volume) of 5.60 hr was obtained. The travel time was confirmed experimentally by conducting a tracer study using NaCl.

Ambient tap water (NO_3^-=15 $mg\,l^{-1}$, pH= 7.15±0.1, I.S.= 40 mM, DO=8±0.2 $mg\,l^{-1}$) was spiked with KNO_3 to reach a total concentration of 130 $mg\,l^{-1}$ NO_3^- and passed through the sand medium for several pore volumes (PVs) to provide a homogeneous, steady state distribution of the contaminated water in the sand medium.

An array of NPRWs was emplaced in three different orientations: vertical ($\hat{\theta} = 90^{\circ}$), horizontal ($\hat{\theta} = 0^{\circ}$), and slanted ($\hat{\theta} = 45^{\circ}$) perpendicular to groundwater flow direction at a distance of 28 cm from the entrance of the model (Fig. 4). Each well in NPRW system is composed by Plexiglass cylinder (inner diameter= 30 mm, outer diameter=40 mm, and length= 250 mm) with numerous openings embedded in its wall, spaced equally along the cylinder. Each well contains a certain amount of NZVI/MZVI mixed with very coarse sand with d_{50}=1.70 mm, ρ_b=1.68 $g\,cm^{-3}$, ρ_s=2.49 $g\,cm^{-3}$, n_{rm}= 0.32, K_{rm}=3.28 $mm\,s^{-1}$ (283.4 $m\,d^{-1}$), and α_L= 5.7 mm to provide adequate hydraulic conductivity contrast between the aquifer medium and reagent materials within wells. Mixing ratio and mass of NZVI and MZVI used in each NPRW were selected based on the results of batch tests.

Two sets of piezometers were placed upstream (UP) and downstream (DP1, DP2, and DP3) the NPRW array, respectively at distance of 15 cm and 45 cm from the model inlet for water sampling. Three downstream piezometers (DP1, DP2, and DP3) were placed in different

depths (Fig. 4) to monitor the treated effluent plume from the NPRWs. The number of wells, distance between wells, and wells diameter for the NPRW array in the bench-scale model were predetermined by numerical simulations using PMPATH (Pollock, 1994) as discussed in section 3.1.

During the experiments, three samples were taken from the upstream (one sample) and downstream (two samples) to obtain the values of NO_3^-, NO_2^-, NH_4^+, EC, pH in the groundwater.

3. Results and Discussion

3.1. Results of Hydraulic Contact Time Computation

Using the flow field solved by groundwater modeling system (MODFLOW) and the semi-analytical particle tracking tool PMPATH (Pollock, 1994), the boundary conditions (constant head for upper and lower boundaries, and no-flow for the other boundaries) and hydraulic properties of bench scale setup, the optimal number of wells in NPRWs system to capture all contaminated groundwater plume was determined to be 6. The diameter of the wells used in the simulations was predefined (0.03 m) according to available Plexiglas cylinders. To delineate the capture zone of the wells, 200 particles were tracked forward by several running the PMPATH from the upstream boundaries while the number of wells were varied in each run. The median length of the streamlines passed through the NPRW (L_{med}) was also estimated from PMDPATH as 0.6 of D_w.

Figure 5 shows the variation of factor f (i.e. W_{cz}/D_w) versus relative hydraulic conductivity (K_R) for a vertical NPRW obtained from Eqs. 8 and 9, and the numerical model PMPATH. The results indicate that by increasing the contrast between the hydraulic conductivity of aquifer and reagent materials within NPRWs (i.e. K_R), more contaminated groundwater

moves through the well. The maximum value of the factor f (i.e. $K_R \rightarrow \infty$) is equal to 2 for Eq. 9, 1.9 for Eq. 8, and 1.85 for PMPATH. The final value of 1.85 for factor f is also reported by Naftz et al. (2002).

Interestingly, the width of the capture zone of NPRW increases with increasing the contrast between K_{rm} and K_{aq} (i.e. K_R) up to 80, but then remains constant for larger values of K_R due to dominant influence of i_R as shown in the Eq. 8. Wiloson et al. (1997) and Freethey et al. (2002) also reported the optimum width of capture zone for a vertical well filled by reactive materials to be 1.8 to 1.9 times of well diameter, when the K_{rm} within reactive materials is 80 to 200 times greater than K_{aq} of aquifer formation adjacent to the well.

Variation of median contact time (t_c) between contaminated plume and reagent material within the NPRW with configurations of horizontal, slanted ($\hat{\theta}$=45°), and vertical for different values of K_R and pore water velocity (V_{aq}) obtained by Eq. 10 are shown in Fig. 6. It is observed that as pore water velocity or relative hydraulic conductivity increases, the hydraulic contact time between contaminated plume and reactive materials decreased exponentially. Horizontal and vertical NPRWs produce the maximum and minimum t_c values, respectively. As the pore water velocity (V_{aq}) or relative hydraulic conductivity (K_R) increases, the effect of NPRW configuration is reduced. The range of pore water velocity in natural aquifers (e.g., 0.08 to 0.8 $m\ d^{-1}$) (Johnson et al., 2009) are shown in Fig. 6 for real-world applications.

The effects of NPRWs orientation (e.g. vertical, horizontal, and slated) on the upgradient capture zone area of the NPRW (a_{cz}) in a homogeneous and isotropic aquifer were also evaluated using the Eq. 12. Figure 7 reports the variations of a_{cz} versus different relative hydraulic conductivity (K_R) in the case that pore water velocity within the aquifer (V) is 0.005 $mm\ s^{-1}$ (0.43 $m\ d^{-1}$), well diameter (D_w) is 0.03 m, and well length (L_w) is 1 m. The results reveal that the vertical orientation of NPRWs (i.e. $\hat{\theta}$=0) yields the maximum area of capture zone. This is a suitable pattern for a large plume of contaminated groundwater which

does not need to be treated completely. On the other hand, horizontal NPRWs can be more suitable for groundwater contaminated by high risk pollutants but with small plume (or thin aquifer). The hydrogeological properties of the aquifer (e.g. type of formation) and practical aspects of well drilling may significantly influence the selection of the appropriate NPRW orientation. A trade-off between the extent of the capture zone (a_{cz}) and the contact time between the contaminated plume and reagent materials (t_c) could be found in a slanted well ($0<\hat{\theta}<90$). Same results could also be obtained (as shown in Fig. 7) for various values of V, D_w, and L_w.

3.2. Results of Batch Experiments

The initial concentrations of NO_3^-, NO_2^-, NH_4^+, EC, pH, and dissolved oxygen (DO) in the solutions of nine treatment were 131±2 $mg\ l^{-1}$, 52 $mg\ l^{-1}$, 0.82 $mg\ l^{-1}$, 570 $\mu S\ cm^{-1}$, 7.15 (±0.1), and 8±0.2 $mg\ l^{-1}$ respectively. The concentration of NO_3^-, NO_2^-, NH_4^+, as well the values of EC, and pH were measured in nine batch tests over time up to 160 h (Table 1 and Fig. 8). The amount of unbalanced nitrogen (N_{ub}) in each time are also calculated by adjusting the mass balance of nitrogen species respect to the initial concentrations as shown in Fig. (8-a) to (8-i).

The trend of nitrate concentration for treatments containing only NZVI (A and B) decreased exponentially, whereas the nitrate reduction rate for treatments C and D (containing only MZVI) followed first order kinetics. Following the exponential nitrate reduction is also valid for other treatments including NZVI (E, F, G, H, and I). This indicates the NZVI outperforms MZVI in NO_3^- reduction (the reaction rate of denitrification through different treatments are discussed in section 3.2.1.). The efficiency of NO_3^- removal increases as the NZVI content of the solution increases (e.g. treatments D and H compared with C) according to the following equation (Su et al., 2014a):

$NO_3^-(aq)+4\ Fe^0(s) + 7\ H_2O \rightarrow 4\ Fe^{2+}(aq) + NH_4^+(aq)+10\ OH^-$

(13)

The nitrate reduction rate in the batch containing only MZVI was slow (treatment C), but almost constant over time. This is consistent with previous findings of Huang et al. (1998), who reported that the rate of nitrate reduction by micro sized Fe^0 is negligible for neutral pH but gradually continues. Conversely, the presence of MZVI along with NZVI has a significant influence on the nitrate reduction (treatment E compared with A) but a slight enhancement in nitrate reduction was observed when the concentration of MZVI was further increased (treatments I and F compared with E). Based on the findings obtained in this study, the stoichiometric ratio of Fe^0-to- NO_3^-, especially when mixing NZVI/MZVI, plays a key role in denitrification process through the batch tests. The minimum half-life time for NO_3^- removal of 40 h was observed for treatments H and A.

During the anaerobic denitrification process by the NZVI/MZVI, nearly all possible forms of N by-products, including NO_3^-, NO_2^-, and NH_4^+ were observed in the solution, with a predominant NH_4^+ production. Flis (1991) reported that the chemical reduction of NO_3^- produces NO_2^-, $N_2(gas)$, and NH_3 depending on the reaction conditions. Agrawal (1997) reported the formation of NH_3 and $N_2(gas)$ and NO_2^- as the major intermediate product during nitrate reduction by ZVI. Choe et al. (2000) reported that $N_2(gas)$ is the only end product of $NO3^-$ reduction by NZVI in anaerobic condition, ambient temperate, and no pH control, whereas NH_3 is the only product of NO_3^- reduction in presence of MZVI (SS=0.063 $m^2\ g^{-1}$). Westerhoff and James (2003) reported that, in the presence of milimetric ZVI and anaerobic conditions, 70% of initial nitrate was converted to ammonium. Yang and Lee (2005) reported that the final products of $NO3^-$ reduction by NZVI in anaerobic condition are NH_4^+ and $N_2(gas)$ without detection of $NO2^-$. In a previous study Hosseini and Tosco (2015)

also reported NH_4^+ and $N_2(gas)$ are the end products of denitrification process by NZVI in anaerobic condition and neutral pH.

In the early stages of reaction (i.e. less than 20 h), a decreasing trend was observed for nitrite concentrations in all treatments (e.g. Fig. 8-b and 8-i). This suggests that the elemental $Fe^0(s)$ can be oxidized to ferrous and ferric following the half-reaction shown in Eqs. (14) and (15) (Cook, 2009). NO_2^- can be reduced to NH_4^+ and maybe to $N_2(gas)$ through the Eqs. (16) and (17) (Hu et al., 1999; Sun et al., 2006):

$$Fe^0(s) \rightarrow Fe^{2+}(aq) + 2e^-(aq) \quad (14)$$

$$Fe^0(s) \rightarrow Fe^{3+}(aq) + 3e^-(aq) \quad (15)$$

$$2NO_2^-(aq) + 8H^+(aq) + 6e^-(aq) \rightarrow N_2(g) + 4H_2O \quad (16)$$

$$NO_2^-(aq) + 8H^+(aq) + 3e^-(aq) \rightarrow NH_4^+(aq) + 2H_2O \quad (17)$$

This study assumed that the reduced mass of nitrite in the early reaction time transforms into ammonium as discussed in the section 3.2.1. The increase in NO_2^- concentration observed after a certain reaction time for all treatments (Fig. 8) could be due to intermediate production of this ion during nitrate reduction (Vavilin and Rytov, 2015). Interestingly, in batch tests containing a high mass of NZVI (e.g. treatments E and H), a delay for the initiation of NO_3^- reduction was observed (compare the concave shape of NO_3^- curves in Fig. 8). This behavior was not observed for treatments containing only MZVI (i.e. treatments C and D). This can be explained assuming that, in aerobic conditions, when adding the NZVI powder to the aqueous solution protons are first reduced by Fe^0 to form atomic hydrogen. This reduced form of hydrogen induces the NO_3^- reduction by Fe^0 or transforms to $H_2(gas)$ according to following reactions (Adeleye et al., 2013):

$$2\,Fe^0(s) + 4H^+(aq) + O_2\,(aq) \rightarrow 2\,Fe^{2+}(aq) + 2H_2O \quad (18)$$

$$Fe^0(s) + 2H_2O \rightarrow Fe^{2+}(aq) + H_2(gas) + 2OH^-\,(aq) \quad (19)$$

The corrosion rate of Fe^0 by water (second reaction) is very slow at neutral pH. The gaseous H_2 may be sorbed at the iron surface as individual hydrogen atom, and act as catalyst to transfer electron and as an inhibitor of further Fe^0 corrosion (Westerhof and James, 2003). A threshold amount of sorbed hydrogen is needed to start the NO_3^- reduction, especially when the dry powder of ZVI was immersed in the solution (Reardon, 1995). This is the responsible mechanism for slow reaction rate or significant lag phase of nitrate removal at the begging of reactions (Alowitz and Scherer, 2002).

According to these findings, a conceptual model is proposed for denitrification process in presence of mixing MZVI/NZVI particles in two stages of early and late of reaction in Fig. 9. According to this conceptual model, the main processes occurring at the NZVI surface in the early stage of reaction include: adsorbing aqueous nitrate, nitrite, and ammonium to the boundary layer of Fe^0 surface, diffusing the adsorbed N species along the boundary layer, chemical reduction of N species by giving electron from Fe, desorption of reduced form of N from Fe surface, production of dissolved hydrogen via cathodic depolarization. In the late stage of reaction the main mechanisms are iron corrosion and formation of non-crystal oxide layer on the Fe surface and therefore decreasing the rate of electron transfer, catalytic reduction of N species by adsorbed hydrogen on the Fe surface, increasing the pH of solution by production of OH^-, and electrostatic repulsion of cathodic N products (e.g. NH_4^+) from iron surface.

In all batch tests, the ammonium concentrations increased over reaction time up to a constant value, which depended on the quantity of Fe^0 dosage used in the solution. Maximum and minimum ammonium production were observed for treatment H and A, respectively equal to 25.8 and 4.6 $mg\ l^{-1}$ at the end of experiment. In all cases, the ammonium concentration remained constant at the end of the increase in solution pH, mostly occurring at 80 h. The kinetics of the ammonium production process is discussed further in the section 3.2.1.

In all treatments, the solution pH rose rapidly from an initial value of 7.15±0.1 to more than 8 after 40 h. The rate of pH increase for batches with mixed NZVI/MZVI (treatments E, F, G, H, and I) was greater than treatments where NZVI or MZVI alone was used (treatments A, B, C, and D).

The connection between NO_3^- removal and increasing pH (as shown in Fig. 8-j) can be described by the high consumption of protons for nitrate reaction (10:1 moles) (Yang and Lee, 2005):

$$NO_3^- + 10H^+ + 4Fe^0 \rightarrow NH_4^+ + 3H_2O + 4Fe^{2+} \quad (20)$$

Additionally, in aerobic conditions, Fe^0 is able to react with dissolved oxygen in water and produces ferrous and hydroxide (Karn et al. 2009):

$$2\,Fe^0(s) + 4H^+(aq) + O_2(aq) \rightarrow 2\,Fe^{2+}(aq) + 2H_2O \quad (21)$$

In anoxic condition, Fe^0 can react with water according to the following equation (Su et al., 2014b):

$$Fe^0(s) + 2H_2O \rightarrow Fe^{2+}(aq) + H_2(g) + 2OH^-(aq) \quad (22)$$

Ferrous ions are further oxidized to ferric ions in the presence of oxygen:

$$4\,Fe^{2+}(aq) + 4H^+(aq) + O_2(aq) \rightarrow 4\,Fe^{3+}(aq) + 2\,H_2O \quad (23)$$

The four above reactions lead to increasing of solution pH. Treatments with higher dose of Fe^0 resulted in a higher increase in pH. At the end of reaction time, the increase in solution pH is negligible due to consuming hydroxyl ions which lead to appearance of greenish suspended rust, inactivation of Fe^0 content, and absence of NO_2^- accumulation (Huang et al., 1998; Choe et al., 2004) as also shown in Fig. 9. A smaller increase in pH in solutions containing MZVI as only reagent (treatments A and B) is linked with the lower denitrification rate of these treatments as discussed before. It is also worth noting that high pH conditions (i.e. high pH) at the end of the tests could stimulate mineral precipitation (e.g. iron hydroxide)

on the Fe^0 surface, and hinder longevity of the reagents by limiting the electron transfer process (see also Fig. 9-b).

An incomplete mass balance of N (i.e. sum of NO_3^-, NO_2^-, and NH_4^+ were less than initial N load) is observed in all treatments. It can be explained by the volatilization of ammonium through transformation into ammonia, production of $N_2(gas)$ and probably $N_2O(gas)$, and sorption of nitrogen products onto the positively charged surface of precipitated iron oxides, especially at high pH conditions (pH> 8) as shown also in Fig. 8. The kind of unbalanced N mass (N_{ub}) in the solutions during the reaction time are not detected in this study.

The electrical conductivity (EC) decreases exponentially in all treatments over time, except those containing only the NZVI (batches A to D). In this case, a decrease in EC is observed after a weak peak for treatments A and B, and later on for treatments C and D. It is evident that the increase in solutions EC is probably due to accumulation of oxided species of iron (i.e. Fe^{2+} and Fe^{3+}) in the solution which generate in higher rates through NZVI. Rapid decreasing of EC could be described by the consumption of nitrate and adsorption/co-precipitation of different ions containing N on the corrosion products of iron (i.e. ferrous and ferric). After a certain time (depends on the Fe^0 content), both the reduction reaction and adsorption reached equilibrium, and therefore EC stabilized (e.g. treatments E, F, and G). These findings consistent with those reported by Tang et al. (2012). A limited increase of EC was observed at the end of the experiments for treatments G and H, which may be due to higher pH conditions of these solutions as shown in Fig. (8-j).

The values of NO_3^-, NO_2^-, NH_4^+, EC, and pH for all treatments at the end of the tests (1200 h) are given in Table (2). For better comparison, the concentrations of these parameters at beginning of experiments are also given in Table (2). The closure N mass balance recovered as NO_3^- (1.9% to 9.4% of initial N), NO_2^- (15% to 18% of initial N), NH_4^+ (14% to 21% of initial N) and N_{ub} (62% to 68% of initial N). Complete NO_3^- removal (98.2%) was obtained

for treatment H, whereas 90% of the initial NO_3^- was reduced for treatment C. The decrease of NO_2^- was in the range 54% to 62% for all treatments. The partial removal is supposed to be due to the competition of this ion with nitrate for its reduction, or to partial sorption onto Fe^0 surface (Siantar et al., 1996).

The long-term concentrations of NH_4^+ (ranged between 18 to 28 $mg\ l^{-1}$) showed a significant increase compared with those observed at a shorter time (e.g. 160 h) when values in the range 4.5 to 26 $mg\ l^{-1}$ were observed. Conversely, the EC did not significantly change over the longer period, compared with values at 160 h. The high pH of solutions tended to rise up slowly of 0.2 (for treatments E to I) to 1.5 pH units (for treatment C), and corresponded always to an increase in NH_4^+ concentration. These findings may be useful in the implications of ZVI fate on the denitrification process for drinking water treatment.

3.2.1. Kinetic Analysis of Nitrate/Nitrite Reduction and Ammonium Stripping

In order to analyze the influence of the micro and nano ZVI particles on the denitrification rate, a kinetic analysis of the NO_3^- and NO_2^- degradation and NH_4^+ production and stripping was conducted on the recorded data during the nine experimental tests. For each operating conditions tested, pseudo first-order kinetic models were used (Liang et al., 2008; Hwang et al., 2011; Hosseini and Tosco, 2013):

$$\frac{dC_{NO_3}}{dt} = -k_1 \cdot C_{NO_3} \tag{24}$$

$$\frac{dC_{NO_2}}{dt} = -k_3 \cdot C_{NO_2} \quad ; \quad for \quad t \le t_1 \tag{25}$$

$$\frac{dC_{NH_4}}{dt} = \begin{cases} k_1 \left(C^0_{NO_3} - C_{NO_3}\right) + k_3\left(C^0_{NO_2} - C_{NO_2}\right) - k_2 \cdot C_{NH_4} & ; \ for \ t \le t_1 \\ k_1 \left(C^0_{NO_3} - C_{NO_3}\right) - k_2 \cdot C_{NH_4} - k_3 \cdot C_{NO_2}; & for \ t > t_1 \end{cases} \tag{26}$$

where $k_1\ [T^{-1}]$, $k_2\ [T^{-1}]$, and $k_3\ [T^{-1}]$ are the constants of nitrate reduction, ammonia stripping, and nitrite reduction, respectively. Dividing the variations of ammonium concentration during time (right hand side of Eq. 26) in two parts is due to the nitrite

reduction occurs in the early time of reaction (i.e. t_1=20 h) and then, nitrite produces in all treatments. Integrating the Eqs. 24 to 26 with respect to time (t), and considering the initial concentrations $C^0_{NO_3}$, $C^0_{NO_2}$, and $C^0_{NH_4}$ as the initial conditions, the function of NO_3^-, NO_2^- (for $t \le t_1$) reduction and NH_4^+ production and stripping during reaction time can be obtained:

Nitrate reduction during reaction time:

$$C^t_{NO_3} = C^0_{NO_3}\, e^{-k_1 t} \tag{27}$$

Nitrite reduction in the early stages of reaction time, $t \le t_1$:

$$C^t_{NO_2} = C^0_{NO_2}\, e^{-k_3 t} \quad ; \tag{28}$$

Ammonium production and stripping by nitrate and nitrite reduction in the early stages of reaction time, $t \le t_1$:

$$C^t_{NH_4} = \frac{k_1}{k_2} C^0_{NO_3} + \left(\frac{k_1}{k_1 - k_2}\right) C^0_{NO_3} e^{-k_1 t} + \frac{k_3}{k_2} C^0_{NO_2} + \frac{k_3}{k_3 - k_2} C^0_{NO_2} \cdot e^{-k_3 t} + \left[C^0_{NH_4} + \left(\frac{{k_1}^2}{{k_2}^2 - k_1 \cdot k_2}\right) C^0_{NO_3} + \left(\frac{{k_3}^2}{{k_2}^2 - k_2 \cdot k_3}\right) C^0_{NO_2}\right] e^{-k_2 t} \tag{29}$$

Ammonium production and stripping by nitrate reduction in late stages of reaction time, $t > t_1$:

$$C^t_{NH_4} = \frac{k_1}{k_2} C^0_{NO_3} + \left(\frac{k_1}{k_1 - k_2}\right) C^0_{NO_3} e^{-k_1 t} + \left[C^0_{NH_4} + \left(\frac{{k_1}^2}{{k_2}^2 - k_1 \cdot k_2}\right) C^0_{NO_3}\right] e^{-k_2 t} \tag{30}$$

where $C^t_{NO_3}$ [ML^{-3}], $C^t_{NO_2}$ [ML^{-3}], and $C^t_{NH_4}$[ML^{-3}] are the aqueous nitrate, nitrite and ammonium concentrations at time t, respectively; $C^0_{NO_3}$, $C^0_{NO_2}$ and $C^0_{NH_4}$ are the initial nitrate, nitrite and ammonium concentrations, respectively. It is noteworthy that the Eqs. The kinetic constants k_1, k_2, and k_3 were optimized by fitting the experimental data of nitrate, nitrite and ammonium concentrations in the batch tests to Eqs. 27 to 30 as shown in Table (3). The increase in solution pH (as shown in Fig. 8-j), and the coating of Fe^0 surface by precipitates may both significantly affect the values of k_1, k_2, and k_3 during the reaction. Consequently in order to obtain a more accurate model estimation of the experimental results, fitting was

performed for different reaction times, separately (Sparis et al., 2013). Regarding the number of measured data, as shown in Fig. (8), the values of k_1 and k_2 for all treatments are obtained for two reaction steps: fast, FRS (up to 45 hr) and slow, SRS (>45 hr). Conversely, the values of k_3 were obtained only for the FRS, since its concentration increased during the SLS. The necessity of calculating the nitrate reduction constants for the two reaction steps in varying pH media was also reported in previous works (e.g. Comba et al., 2012). The results of fitted k_1, k_2, and k_3 values are presented in Table (3). The significant agreement between the experimental results and theoretical predictions (R^2 values in Table 3) indicates a good validation of the proposed kinetic models, which is consistent with the findings of other authors (e.g. Liou et al., 2005; Hwang et al., 2011; Hosseini et al., 2015, Sparis et al., 2013).

Results show that the k_1 value of the FRS in the solution containing NZVI (treatments A and B) was averagely more than 3 folds greater than that calculated for the SRS. Conversely, this increase was averagely 1.5 folds in the solutions containing MZVI (treatments C and D). A decrease of nitrate reduction rate (k_1) during the last period is also reported by previous researches (e.g. Hwang et al., 2011; Comba et al., 2012). Results also indicate that the k_2 value of the FRS was averagely more than 16 folds greater than that calculated for the SRS, mainly due to the reduction of nitrates and nitrites to ammonium (according to Eqs. 17 and 20).

The minimum kinetic nitrate, nitrite reduction and stripping constants (k_1, k_2, and k_3) were obtained for treatments C and D (containing only the MZVI), while the maximum values of these constant were obtained for treatments A, B, and H (containing the maximum NZVI). The abatement curves of nitrite and nitrate (during the SRS) generally showed faster decreasing trends (i.e. higher values of k_1 and k_3) with the Fe^0 dosage used in the solution. The values of k_1 (0.002 to 0.16 h^{-1}) and k_2 (0.008 to 0.10 h^{-1}) during the SRS are consistent with previous works. For example, Hosseini and Tosco (2015) obtained values of k_1 and k_2

equal to 0.29 and 2.29 day^{-1} (0.012 and 0.095 h^{-1}) for nitrate reduction (with initial concentration of 105 $mg\ l^{-1}$) by NZVI (4 $g\ l^{-1}$) in batch tests in anaerobic conditions and neutral pH. Nevertheless, the obtained k_1 values in this study are much smaller than ones reported in some studies. Choe et al. (2000) reported the rate constant of nitrate reduction by NZVI (SS=31.4 m^2g^{-1}) between 214 to 224 day^{-1} (8.92 to 9.33 h^{-1}) in ambient conditions. Sianter et al. (1996) reported a rate constant of reaction of 300±57 day^{-1} (12.5± 2.5 h^{-1}) under anaerobic NO_3^- reduction in buffered solution (with pH~7) by micro Fe^0. Hwang et al. (2011) reported the k_1 value between 6.30 to 6.60 h^{-1} for the buffered solution containing 100 $mg\ l^{-1}$ nitrate and 1250 $mg\ l^{-1}$ NZVI for the first 15 min of reaction time. Sparis et al. (2013) obtained the k_1 value equal to 1.52 h^{-1} for the buffered solution containing 200 $mg\ l^{-1}$ nitrate and 3330 $mg\ l^{-1}$ NZVI for the first 20 min of reaction time. Difference in selecting the time of changing reaction constant may be the reason of obtained small values of k_1 in this study (i.e. 45 h).

It is noteworthy the effect of increasing mass of reagents (NZVI or MZVI) on the kinetic constants of k_1 and k_2. The effect of the used amount of nano-sized ZVI on the nitrate and ammonium stripping kinetics is greater than micro-sized ZVI, especially during the SRS. For a given MZVI concentration (e.g. 2 $g\ l^{-1}$), adding a constant mass of NZVI to the solution (e.g. 2 $g\ l^{-1}$ in treatments D and H) results in an increase of 3.8 times (from 0.004 to 0.016 h^{-1}) for k_1 and 1.9 times (0.0087 to 0.0169 h^{-1}) for k_2. Conversely, adding 2 $g\ l^{-1}$ MZVI to the solution containing 0.5 $g\ l^{-1}$ NZVI (treatments A and F), results only an increasing 1.75 times for k_1 (0.008 to 0.014 h^{-1}) and 1.73 for k_2 (0.006 to 0.010 h^{-1}).

3.3. Nitrate Removal through NPRWS

Based on the results of batch tests and also numerous pretests conducted in the bench scale sand medium experiments, each NPRWs containing 2 g NZVI, 10 g MZVI, and 120 g very

coarse sand. This resulted in relative hydraulic conductivity K_R=4, and therefore the factor f will be 1.48 according to Fig. 5. Results of numerical simulations by PMPATH reproducing the experimental setup indicated that six wells (with inner and outer diameters 0.03 and 0.04 m, respectively) are suitable to capture all upstream groundwater plume (as also shown in Fig. 4). The concentrations of NO_3^-, NO_2^-, NH_4^+, EC, and pH in the upstream (UP) and downstream piezometers (DP1 to DP3) were measured every 10.0 h (i.e. every pore volume time) for up to five pore volumes, and are shown in Fig. 10. The monitored nitrogen species and EC in the effluent groundwater of vertical NPRWs have the same values for three downstream piezometers (DP1 to DP3), since the vertical wells collect all the upstream contaminated plume. Conversely, the horizontal and slanted NPRWs (with inclined angle of $\hat{\theta}$=45°) cover 25% and 75% of the contaminated plume, respectively. In the horizontal NPRWs, only the piezometer DP2 monitored water treated in the wells, while water collected at the piezometers DP1 and DP3 was not intercepted by the wells (see also Fig. 4).

For the vertical NPRWs, the influent concentration of NO_3^- (i.e. 128 $mg\ l^{-1}$) was reduced down to 36% of the initial value in the first two PVs, and then increased (Fig. 10-a). Conversely, the NO_3^- removal for the horizontal (monitored in piezometer DP2) and slanted NPRWs (average of three downstream piezometers) was 79% and 41% of the influent NO_3^-, respectively.

During each bench scale experiments (i.e. five PVs), approximately 50 litres of contaminated groundwater passed through the NPRWs, resulting in a ratio of Fe^0-to-NO_3^- equal to 5.85 $g\ g^{-1}$. The amount of Fe^0 present in the NPRWs is comparable with those used in the batch tests (i.e. treatments A and B as shown in Table 1). Moreover, the inflow provided continuously newly contaminated water, compared to the batch tests. These are the reasons why the effluent nitrate concentration for the NPRWs increases after a certain number of PVs. As a general rule, the nitrate removal rate for the slanted NPRWs was significantly lower than

for the two other NPRWs. Effluent NO_2^- and NH_4^+ concentrations for three NPRWs orientations increased during the experimental time but in different extents. The maximum increase in nitrite and ammonium were observed in the horizontal NPRWs (in piezometer DP2) and slanted NPRWs, respectively (10-d to 10-i). This reveals that the effluent concentrations of these ions are directly related to the contact time of contaminant plume with the reagents through the NPRWs.

The EC of effluent solution from three NPRWs systems increased up to a certain value (due to production of ions through nitrate reduction process) and then remained constant (in horizontal NPRWs) or decreased (in vertical and slanted NPRWs) as shown in Fig. (10-j) to (10-o). This behavior can be also explained by the refreshing of influent plume to the NPRWs by groundwater with less EC. An increase of the EC values in the effluent solution of vertical NPRWs containing the NZVI/coarse sand was not observed in the previous work (Hosseini and Tosco, 2015), likely due to the different water chemistry used in the experiments. Variations of solution pH in the effluent rose up and then decreased similarly to the trend of NO_3^- and EC. It should be mentioned that nitrate removal process through the NPRWs filled by micro/nano Fe^0 accompanied by NO_2^- and NH_4^+ production, proton consumption (i.e. increasing pH), and increasing the EC of effluent solution which was stimulated by the slanted orientation of wells.

A minor reduction of the permeability of the filling materials in the NPRWs was observed after completing the experiments, likely because the pH of the medium was not sufficiently high (<8) to allow significant precipitation of iron oxyhydroxide (FeOOH), which was reported in previous works (e.g. Gandhi et al., 2002).

Denitrification processes in batch and bench-scale experiments indicated conformity in the closure N products (i.e. NO_2^-, NH_4^+, and $N_2(g)$), but comparing the N mass balance between two experiments is not possible due to differences in experimental conditions. In the

bench sand medium tests, the DO has a significant impact on the nitrate removal process through the NPRWs systems than the batch tests due to refreshing DO content in recycling contaminated water.

After the experiments, the remained mass of MZVI and NZVI particles in each NPRW was also measured by weighting the dried contains of each NPRW (sand, MZVI, and NZVI). Averagely, 8% (~ 1.0 g) mass loss is observed in each well. This implies that the amount of NZVI and MZVI that leached out of each NPRW to the aquifer (the initial mass of NZVI and MZVI in each well is 12.0 g), since the containing coarse sand in the wells can't be passed through the opening embedded along the cylinder wall. However, the NZVI particles are stabilized by a thin layer of iron oxide, but insignificant mass of these particles are leached out the NPRW.

3.4. Synthesis of Experimental and Modeling Results

The connection between analytical equations (i.e. Eqs. 12, 14, and 16), batch and sand-box experiments can be established by coupling the hydraulic contact time (t_c) between contaminant plume and reagents through a NPRWs system (Eq. 10) and the pseudo first-order kinetic model (Eq. 23) for nitrate reduction by the reagent used in the NPRWs. Combining these equations yields the percentage of nitrate reduction rate (PNR) through each NPRW with different inclination angle $\hat{\theta} \in [0, 90^{\circ}]$ during the time t_c as follows:

$$PNR = \left(1 - \frac{C^{t_c}}{C_0}\right) \times 100 = (1 - e^{-k_1 \times t_c}) \times 100 \qquad (25)$$

where C_0 and C^{t_c} are the nitrate concentrations in upstream and downstream plume of NPRWs, respectively. Other parameters are defined earlier. Computing the values of t_c within the vertical, slanted, and horizontal NPRWs using the Eq. 14, and considering the

values of k_1 for treatments A (as lower limit) and B (as upper limit) during the SRS in the batch experiments (i.e. k_1=0.008 to 0.010 hr^{-1}), the variations of PNR can be obtained using the Eq. 29. The values of t_c are obtained 380 s, 537 s, and 4219 s respectively for vertical, slanted (with $\hat{\theta}$=45°), and horizontal NPRW. The results obtained using analytical Eq. 25 and the measured values of PNR through NPRWs systems in three orientations of vertical, slanted, and horizontal wells are shown in Fig. 11.

The developed analytical equations can simulate the mean value of PNR observed in the sand-box experiments (as indicates by open circles in Fig. 11) in the horizontal NPRW, and low values of PNR in the slanted and vertical NPRWs. However, the higher values of observed PNRs in three configurations of NPRW are not enclosed by the analytical solution domain.

4. Conclusion

The efficacy of non-pumping reactive wells (NPRWs) system in three orientations of vertical, slanted (with inclination angle $\hat{\theta}$=45°), and horizontal for the degradation of nitrate-contaminated groundwater was assessed through laboratory bench-scale studies and modelling. The reactive material emplaced in the wells was a mixture of nano/micro Fe^0 which was selected based on several batch tests. The delineation of steady state capture area for NPRWs, the optimal spacing among the NPRWs and number of wells in the bench-scale model were designed based on flow simulations using the semi-analytical particle tracking model, PMPATH, whereas the aquifer is assumed to be a homogeneous and isotropic medium. The results obtained in this study can be summarized as follows:

1) Emplacing the mixture of nano/micro Fe^0 and sand as a reducing agent in non-pumping reactive wells (NPRWs) is a promising technology for remediation of deep groundwater

contaminated by NO_3^-. This approach incorporates both advantages of high reactivity of NZVI and slow but continuous reactivity of MZVI to ensure the longevity and efficiency of the denitrification process in the field scale.

2) The presence of the NZVI in the reactive medium not only contributes directly to the NO_3^- reduction in early reaction time, but also stimulates the denitrification rate by MZVI through production of hydrogen which acts as catalyst to electron transfer.
3) Despite efficiency of MZVI and NZVI in nitrate reduction, the possible generation of toxic by-products and greenhouse gases (e.g. ammonium and N_2O) may be a limitation of these reagents.
4) Closure N products of denitrification process by nano and micro ZVI in batch tests and bench-scale experiments were NO_2^-, NH_4^+, and unbalanced nitrogen products (probably gaseous N_2).
5) Based on the results of batch tests, the rate of NO_3^- removal increases as the mass of Fe^0 content in the solution increases. However, using additional mass of Fe^0 in the NPRWs may increase the nitrate removal rate, but would likely decrease the hydraulic conductivity of the reactive medium by precipitation of iron oxides in long-term operations.
6) The results of the numerical model PMPATH indicated that for a homogeneous and isotropic aquifer a maximum capture width of 1.85 times greater than the NPRW diameter is obtained for relative hydraulic conductivity K_R=4. Increasing the K_R (>80) does not have a significant effect on the width of the capture zone.
7) A trade-off between the hydraulic conductivity of reactive materials, mass of Fe^0 used in the NPRWs, and orientation of NPRWs should be considered to increase the capture area of wells from upgradient contaminated plumes and also nitrate removal rates.

8) The hydraulic contact time of influent contaminated plume with reagent materials can be controlled by tuning the inclination angle of NPRWs with respect to groundwater flow direction.
9) Horizontal NPRWs filled by reactive materials provide adequate hydraulic contact time between the contamination and reagent materials and are applicable for the remediation of groundwater plume with limited size and dimensions (or thin aquifers) contaminated by high risk and toxic pollutants which need to be completely attenuated. A higher efficiency of the horizontal NPRWs can be obtained when groundwater velocity has a significant vertical component. Additionally, implementing the low reactivity and time consuming degradation mechanism (e.g. biodegradation) can be also operated in the horizontal NPRWs.
10) The vertical NPRWs system is appropriate for remediation of deep contaminated groundwater where moderate degradation is needed. However, the efficiency of vertical NPRWs for pollutant degradation can be enhanced by drilling more consecutive arrays of wells. Slanted NPRWs system is an appropriate choice for treatment of deeply extended contamination plume, as well the degree of pollutant degradation can be managed by changing the inclination angle of wells.
11) Concentrating the reactive materials (i.e. NZVI and MZVI) in the NPRW system may reduce the risk of particle release in the environment over long-time frames, even if the mobility of bare (non-stabilized) NZVI is very limited under natural flow conditions.
12) Pivotal issues including heterogeneity of aquifer media, transient nature of groundwater hydraulics and geochemistry should be considered in the design and up-scaling of NPRWs system as a remediation systems from batch, to laboratory, and then to pilot scale.

The authors are aware that this practical approach makes more complicated the full comprehension of the reaction mechanisms occurring in the batch and the bench scale model, but provides more reliable results for the up-scaling of the technology to the field. The main focus of this study was to modify the hydraulic contact time of nitrate with reagents (i.e. NZVI/MZVI), and area of well capture zone by changing the orientations of NPRWs, while other affected factors (e.g. initial pH, initial DO, and initial NO_3^-, pore water velocity, aquifer medium) were considered constant. More studies to investigate the effects of these factors on the efficiency of NPRWs with different orientations are useful future research directions. Furthermore, tracking different kinds of N byproducts in the solutions, especially associated with the production of greenhouse gasses (e.g. N_2O), during the reaction time of nitrate with ZVI is strongly suggested for the future studies.

5. Nomenclatures

Ar	Argon gas
DO	Dissolved Oxygen
DP	Downstream piezometer
EC	Electrical Conductivity
HCT	Hydraulic contact time
Fe	Iron
MZVI	Micro zero-valent iron
NZVI	Nano zero-valent iron
NPRW	Non-pumping reactive well
FeOOH	Oxyhydroxide
PNR	Percentage of nitrate reduction rate
PRB	Permeable reactive barrier
PVs	Pore volumes
PMPATH	Semi-analytical particle tracking model
NaCl	Sodium Chloride

SS [L^2]	Specific surface
TDS	Total Dissolved Solids
UP	Upstream piezometer
ZVI	Zero-valent iron
pH	Acidity
e	Euler's number
f [-]	Proportion of width of capture zone to the well diameter
t [T]	Time
$\hat{\theta}$ [degree]	Inclination angle of well respect to vertical axis
k_2 [T^{-1}]	Ammonia stripping constant
NH_4^+	Ammonium
$C_{NH_4}^t$[ML^{-3}]	Aqueous Ammonium concentrations at time t
$C_{NO_3}^t$ [ML^{-3}]	Aqueous nitrate concentrations at time t
a_{cz} [L^2]	Area of capture zone
ρ_b [ML^{-3}]	Bulk density of soil
t_c [T]	Contact time between the contaminant plume and reactive agents
R^2 [-]	Determination coefficient
Q_{rm} [L^3T^{-1}]	Discharge through the reactive material
Q_{cz} [L^3T^{-1}]	Discharge through the upgradient capture zone of the NPRW
K_{aq} [LT^{-1}]	Hydraulic conductivity of aquifer material
K_{rm}[LT^{-1}]	Hydraulic conductivity of reactive material
i_{aq} [-]	Hydraulic gradient of aquifer
i_{rm} [-]	Hydraulic gradient of reactive materials
H_2	Hydrogen gas
$C_{NO_3}^0$ [ML^{-3}]	Initial Ammonium concentration
$C_{NO_3}^0$ [ML^{-3}]	Initial nitrate concentration
$L_w[L]$	Length of well
α_L [L]	Longitudinal dispersivity
d_{50} [L]	Mean diameter of soil
L_{med} [L]	Median flow path through the NPRW
NO_3^-	Nitrate
k_1 [T^{-1}]	Nitrate reduction constant

NO_2^-	Nitrite
k_3 [T^{-1}]	Nitrite reduction constant
	N Nitrogen gas
ρ_s [ML^{-3}]	Particle density of soil
V_{aq} [LT^{-1}]	Pore water velocity through aquifer
V_{rm} [LT^{-1}]	Pore water velocity through reactive materials
n_{aq} [-]	Porosity of aquifer
n_{aq} [-]	Porosity of aquifer materials
n_{rm} [-]	Porosity of reactive materials
n_{rm} [-]	Porosity of reactive materials
K_R [-]	Relative hydraulic conductivity
i_R [-]	Relative hydraulic gradient
V_R [-]	Relative pore water velocity
n_R [-]	Relative porosity
N_t	Total nitrogen
N_{ub}	Unbalanced nitrogen
$D_w[L]$	Well diameter
W_{CZ} [L]	Width of capture zone of well

6. References

Adeleye, A.S., Keller, A.A., Miller R.J., and Lenihan, H.S., 2013. Persistence of commercial nanoscaled zero-valent iron (nZVI) and by-products. Journal of Naoparticle Research, 15, 1418. DOI 10.1007/s11051-013-1418-7

Agrawal, A., Tratnyek, P.G., 1996. Reduction of nitro aromatic compounds by zero-valent iron metal. Environmental Science & Technology 30(1), 153–160.

Alowitz, M.J., and Scherer, M.M., 2002. Kinetics of nitrate, nitrite, and Cr (VI) reduction by iron metal, Environ. Sci. Technol. 36, 299–306.

Bear, J., 1979. Hydraulics of Groundwater, McGraw-Hill series in water resources and environmental engineering, McGraw-Hill International Book Co., London ; New York, xiii, 567 p. pp.

Choe, S., Chang, Y.Y., Hwang, K.Y., and Khim, J., 2000. Kinetics of reductive denitrification by nanoscale zero-valent iron. Chemosphere 41, 1307–1311.

Choe, S., Liljestrand, H.M., and Khim, J., 2004. Nitrate reduction by zero-valent iron under different pH regimes. Applied Geochemistry 19, 335–342.

Comba, S., Martin, M., Marchisio, D., Sethi, R., and Barberis, E., 2012. Reduction of nitrate and ammonium adsorption using microscale iron particles and zeolitite. Water Air Soil Pollut, 223, 1079–1089. DOI 10.1007/s11270-011-0926-2

Day, S.R., S.F. O'Hannesin, and L. Marsden., 1999. Geotechnical techniques for the construction of reactive barriers. Journal of Hazardous Materials 67, 285–297.

Della Rocca, C., Belgiorno, V., and Meriç, S., 2007. Overview of in-situ applicable nitrate removal processes. Desalination 204, 46–62.

Flis, J., 1991. Stress corrosion cracking of structural steels in nitrate solutions. In: Corrosion of Metals and Hydrogen- Related Phenomena. Materials Science Monograph. Vol. 59. Amsterdam: Elsevier Science Publishers, 57–94.

Freethey, G.W., Naftz, D.L., Rowland, R.C., Davis, J.A., 2002. Deep aquifer remediation tools: theory, design, and performance modeling. In: Naftz, D.L.,Morrison, S.J., Davis, J.A., Fuller, C.C. (Eds.), Handbook of Groundwater Remediation Using Permeable Reactive Barriers. Academic Press, Amsterdam, pp. 133–161.

Gandhi, S., Oh, B., Schnoor, J.L., and Alvarez, P.J., 2002. Degradation of TCE, Cr(VI), sulfate, and nitrateconsum mixtures by granular iron in flow-through columns under different microbial conditions. Water Research 36, 1973–1982.

Grieger, K.D., Fjordbøge, A., Hartmann, N.B., Eriksson, E., Bjerg, P.L., and Baun, A., 2010. Environmental benefits and risks of zero-valent iron nanoparticles (nZVI) for in situ remediation: Risk mitigation or trade-off? Journal of Contaminant Hydrology 118, 165–183.

Hantush, M.S., and Papadopulos, I.S., 1962. Flow of ground water to collector wells, J. Hydraul. Div. Proc. Am. Soc. Civ. Eng., HY5, 221–244.

Hosseini, S.M., and Tosco, T., 2013. Transport and retention of high concentrated nano-Fe/Cu particles through highly flow-rated packed sand column, Water Research 47, 326-338.

Hosseini, S.M., and Tosco, T., 2015. Integrating NZVI and carbon substrates in a non-pumping reactive wells array for the remediation of a nitrate contaminated aquifer, Journal of Contaminant Hydrology 179, 182-195.

Hosseini, S.M., Ataie-Ashtiani, B., and Kholghi, M., 2011a. Bench scaled nano-Fe0 permeable reactive barrier for nitrate removal. Journal of Groundwater Monitoring and Remediation 31(4), 82-94. DOI: 10.1111/j1745–6592.2011.01352.

Hosseini, S.M., Ataie-Ashtiani, B., and Kholghi, M., 2011b. Nitrate reduction by nano-Fe/Cu particles in packed sand column, Journal of Desalination 276, 214–221, DOI:10.1016/j.desal. 2011.03.051.

Hu, H.Y., Iwasaki, K.F., Goto, N., Kasakura, T., He, Y.M., and Tsubone, T., 1999. Chemical reduction of nitrate and nitrite in aquatic solution by zero-valent metals. Proc. 7th IAWQ Asia-Pacific Regional Conf. Taipei, Taiwan 1, 553–558.

Huang, C.P., Wang, H.W., and Chiu, P.C., 1998. Nitrate reduction by metallic iron. Water Research 32(8), 2257-2264.

Huang, C.S., Chen, Y.L., and Yeh, H.D., 2011. A general analytical solution for flow to a single horizontal well by Fourier and Laplace transforms, Adv Water Resour. 34, 640-648. DOI 10.1016/j.advwatres.2011.02.015.

Hwang, Y.H., Kim, D., and Shin, H., 2011. Mechanism study of nitrate reduction by nano zero valent iron. Journal of Hazardous Materials 185, 1513–1521.

Johnson, R., Johnson, G.O., Nurmi, J., and Tratnyek, P.G., 2009. Natural organic matter enhanced mobility of nano zerovalent iron. Environ. Sci. Technol. 43, 5455–5460.

Kompani-Zare, M., Zhan, H., and Samani, N., 2005. Analytical study of capture zone of a horizontal well in a confined aquifer. J Hydrol. 307, 48–59.

Liang, X., Zhan, H., Zhang, Y.K., and Li,u J., 2016. On coupled unsaturated-saturated low process induced by vertical, horizontal and slant wells in unconfined aquifers. Hydrol. Earth Syst. Sci. Discuss., doi:10.5194/hess-2016-481.

Liang, F., Fan, J., Guo, Y., Fan, M., Wang, J., and Yang, H., 2008. Reduction of Nitrite by Ultrasound-Dispersed Nanoscale Zero-Valent Iron Particles. Ind. Eng. Chem. Res. 47, 8550–8554. DOI: 10.1021/ie8003946

Liou, Y.H., Lo, S.L., Lin, Ch.J., Kuan, W.H., and Weng, Sh.Ch., 2005., Chemical reduction of an unbuffered nitrate solution using catalyzed and uncatalyzed nanoscale iron particles, J. Hazard. Mater. 127, 102–110.

Ludwig, T., and Jekel, M., 2007. Copper and zinc removal from roof runoff in an iron-corrosion system. Vom Wasser, 107, 15–19.

Morgan, J.H., 1992. Horizontal drilling applications of petroleum technologies for environmental purposes, Ground Water Monit. Rem. 12(2), 98– 102.

Naftz, D.L., Morrison, S.J., Davis, J.A., and Fuller, C.C., 2002. Handbook of Groundwater Remediation Using Permeable Reactive Barriers, Applications to Radionuclides, Trace Metals, and Nutrients. Academic Press, San Diego, CA.

Painter, B.D.M., 2004. Reactive barriers: Hydraulic performance and design enhancements. Ground Water 42(4), 609–617.

Pollock, D.W., 1994. User's guide for MODPATH/MODPATH-PLOT, version 3: a particle tracking post-processing package for MOD-FLOW, the U.S. Geological Survey finite-difference ground-water flow model. US Geological Survey Open-File Report 94-464, 249 pp.).

Puls, R.W., Blowes, D.W., and Gillham, R.W., 1999. Long-term performance monitoring for a permeable reactive barrier at the U.S. Cpast Guard Support Center, Elizabet City, North Carolina. Journal of Hazard Materials 68(1), 109-124.

Reardon, E.J., 1995. Anaerobic corrosion of granular iron: Measurement and interpretation of hydrogen evolution rates. Environmental Science & Technology 29(12), 2936–2945.

Sawyer, C.S., and Lieuallen– Dulam, K.K., 1998. Productivity comparison of horizontal and vertical ground water remediation well scenarios, Ground Water 36(1), 98–103.

Schafer, D.C., 1996. Determining 3D capture zone in homogeneous, anisotropic aquifers. Ground Water 34(4), 628-639.

Siantar, D.P., Schreier, C.G., Chou, S.S., and Reinhard, M., 1996. Treatment of 1, 2-dibromo-3-chloropropane and nitrate-contaminated water with zero-valent iron or hydrogen/ palladium catalysts, Water Research 30(10), 2315-2322.

Sparis, D., Mystrioti, Ch., Xenidis, A., and Papassiopi, N., 2013. Reduction of nitrate by copper-coated ZVI nanoparticles. Desalination and Water Treatment, 51(13-15), 2926-2933. DOI: 10.1080/19443994.2012.748303

Su, Y., Adeleye, A.S., Ch., Zhou, X., Dai, Zhang, W., Keller, A.A., and Zhang, Y., 2014b. Effects of nitrate on the treatment of lead contaminated groundwater by nanoscale zerovalent iron. Journal of Hazardous Materials 280, 504–513.

Su, Y., Adeleye, A.S., Huang, Y., Sun, X., Dai, Ch., Zhou, X., Zhang, Y., and Keller, A.A., 2014a. Simultaneous removal of cadmium and nitrate in aqueous media by nanoscale zerovalent iron (nZVI) and Au doped nZVI particles. Water Research, 63, 102-111.

Tang, C., Zhang Z., and Sun X., 2012. Effect of common ions on nitrate removal by zero-valent iron from alkaline soil. Journal of Hazardous Materials 231– 232, 114– 119.

Tratnyek, P.G., Scherer, M.M., Johnson, T.J., and Matheson, L.J., 2003. Permeable reactive barriers of iron and other zero-valent metals. In: Tarr, M.A. (Ed.), Chemical Degradation Methods forWastes and Pollutants: Environmental and Industrial Applications. Marcel Dekker, New York, pp. 371–421.

Tsou, P.R., Feng, Z.Y., Yeh, H.D., and Huang, C.S., 2010. Stream depletion rate with horizontal or slanted wells in confined aquifers near a stream. Hydrol. Earth Syst. Sci. 14, 1477–1485.

United States Environmental Protection Agency, USEPA, 1998. Permeable Reactive Barrier Technologies for Contaminant Remediation. Report EPA/600/R-98/125, USEPA Office of Solid Waste and Emergency Response, Washington DC. [Available through: http://clu-in.org].

Vavilin, V.A., and Rytov, S.V., 2015. Nitrate denitrification with nitrite or nitrous oxide as intermediate products: Stoichiometry, kinetics and dynamics of stable isotope signatures. Chemosphere. 134, 417-426. Doi: 10.1016/j.chemosphere.2015.04.091

Westerhoff, P., and James, J., 2003. Nitrate removal in zero-valent iron packed columns. Water Research 37(8), 1818-1830.

Wheatcraft, and Winterberg, F., 1985. Steady State Flow Passing Through a Cylinder of Permeability Different From the Surrounding Medium. Water Resources Research 21(12), 1923-1929.

Wilkin, R.T., Puls, R.W., and Sewell, G.W., 2002. Long-term performance of permeable reactive barriers for ground water remediation: An evaluation at two sites. U.S. EPA Environmental Research Brief, U.S. EPA/600/S-02/001.

Wilson, R.D., Mackay, D.M., and Cherry, J.A., 1997. Array of un-pumped wells for plume migration control by semi-passive in-site remediation. Groundwater Monitoring and Remediation Journal 17(3), 185-193.

Yang, G.C.C. and Lee, H.L., 2005. Chemical reduction of nitrate by nanosized iron: kinetics and pathways. Water Research 39, 884–894.

Yeh, H.D., and Chang, Y.C., 2013. Recent advances in modeling of well hydraulics, Adv Water Resour 51, 27-51, DOI: 10.1016/j.advwatres.2012.03.006.

Young, G.K., Bungay, H.R., Brown, L.M., and Parsons, W.A., 1964. Chemical reduction of nitrate in water. J. Water Pollut. Control Federation 36, 395–398.

Zhan, H., and Zlotnik, V.A., 2002. Ground water flow to horizontal and slanted wells in unconfined aquifers. Water Resour Re. 38 (7), 1108-1121.

7. Figures

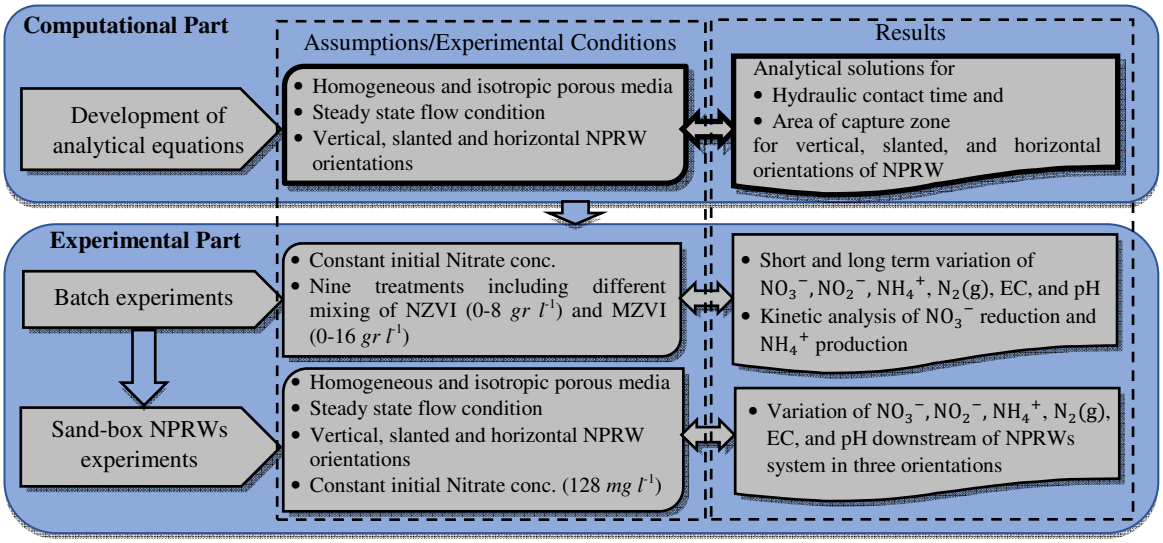

Fig. 1. Schematic diagram of different parts of research in this study.

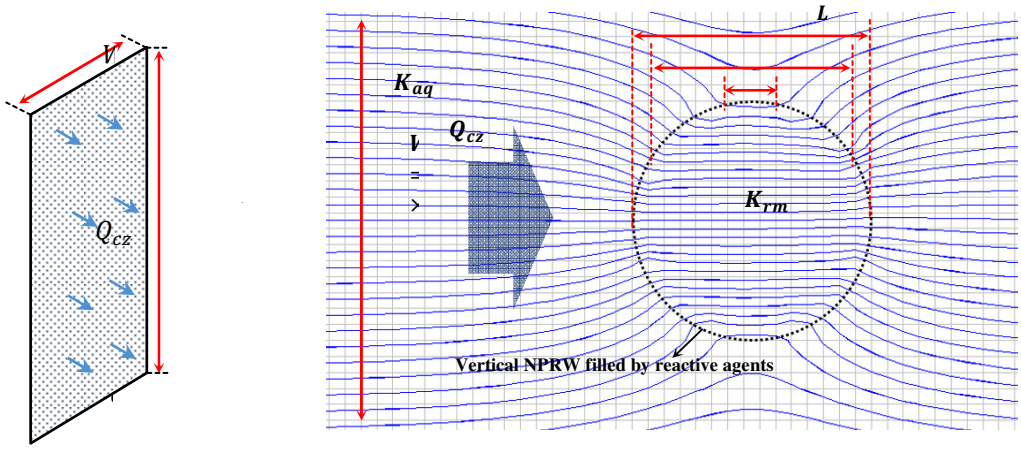

Fig. 2. Steady state capture area for a vertical NPRW filed by reactive materials simulated by PMPATH using tracking 200 particles and hydraulic conductivity contrast K_{rm}/K_{aq} =80 (K_{aq} and K_{rm} are the hydraulic conductivity of aquifer media and reactive materials within the NPRW, respectively). For this case, the width of well capture zone (W_{cz}) is equal to 1.85D_w (i.e. f=1.85).

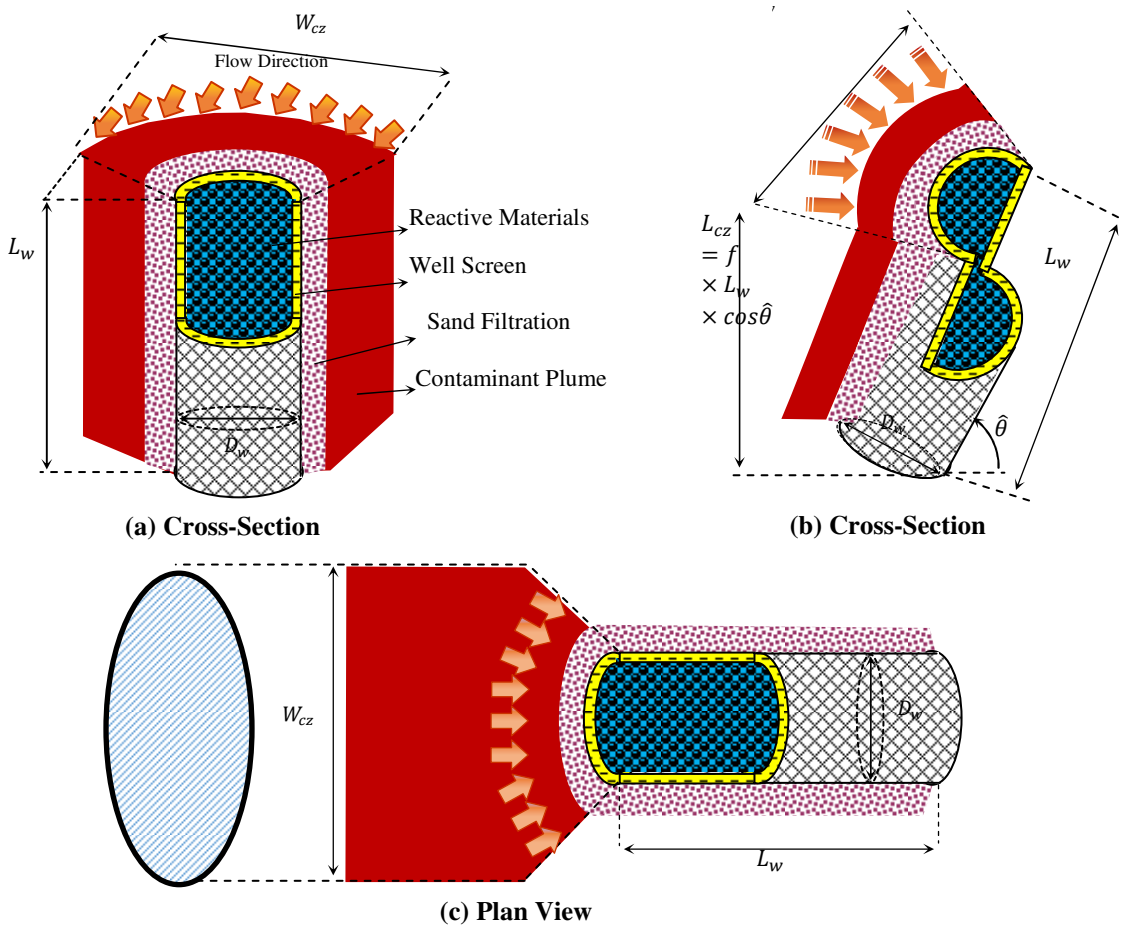

Fig. 3. Schematic of a non-pumping reactive well (NPRW) and the parameters used for contact time and area of capture zone (equations 1 and 2) in three conditions of a) vertical ($\hat{\theta}$ =90), b) slanted with inclination angle $\hat{\theta}$, and c) horizontal ($\hat{\theta} = 0^{\circ}$).

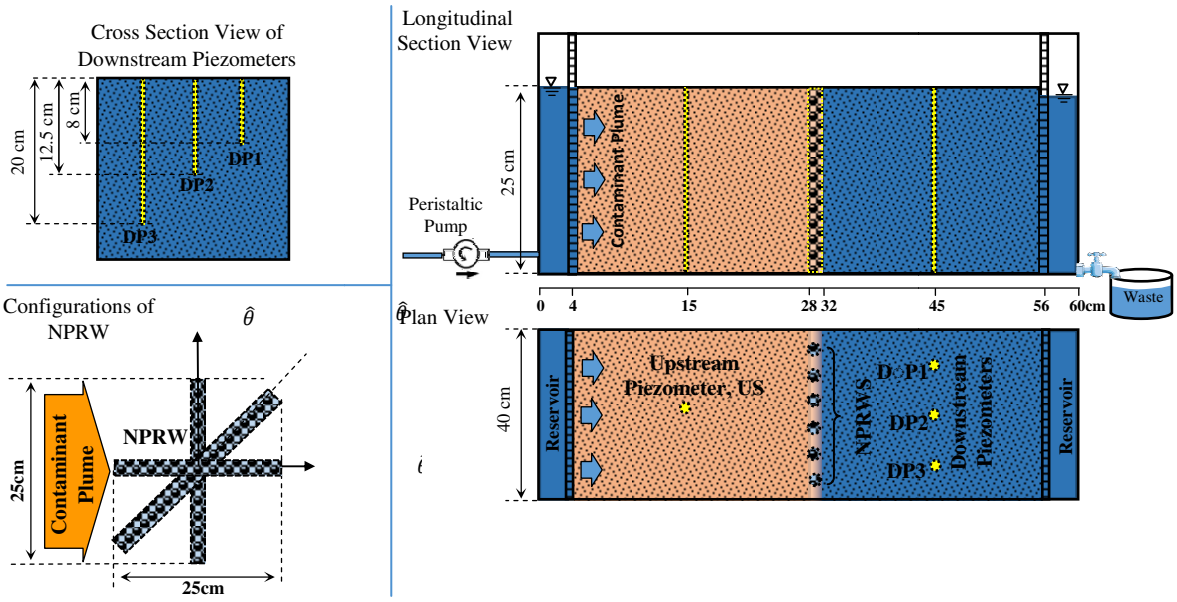

Fig. 4. Schematic of bench-scale setup.

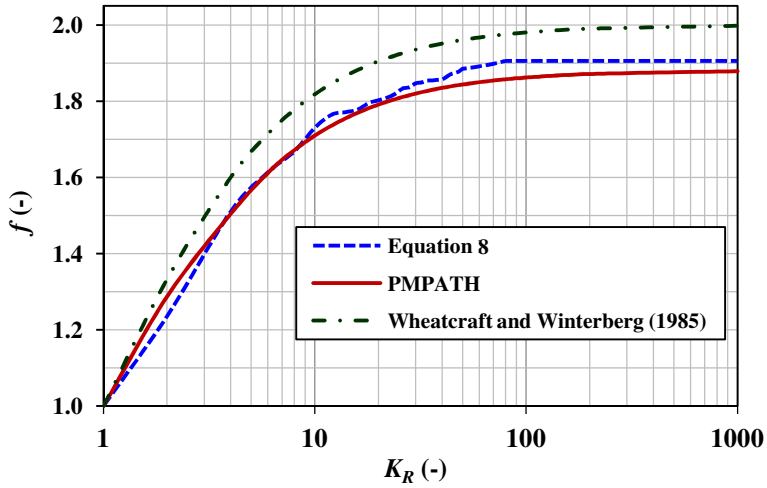

Fig. 5. Variation of factor f ($f = W_{cz}/D_w$) for a vertical NPRW versus relative hydraulic conductivity, K_R: estimated by equation (8), equation proposed by Wheatcraft and Winterberg (1985) (equation 9), and numerical model PMPATH (using tracking forward 200 particles from the upstream boundaries).

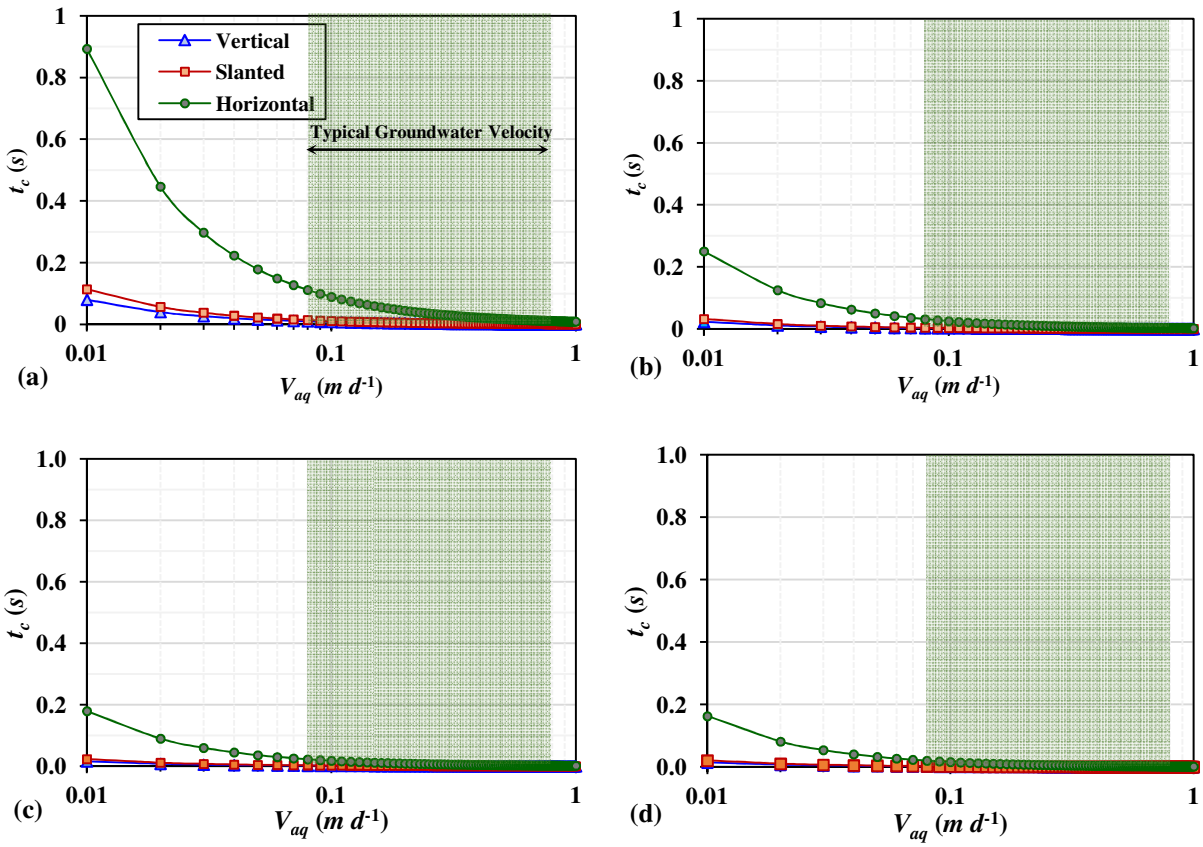

Fig. 6. Variation of mean contact time (t_c) in a vertical, slanted ($\hat{\theta}$=45°), and horizontal NPRW versus pore water velocity of water through homogeneous and isotropic aquifer (Equation 10). The relative hydraulic conductivity is a) K_R=1, b) K_R=2, c) K_R=10, and d) K_R=100. In all cases well diameter D_w=0.03 m, and well length L_w=1 m.

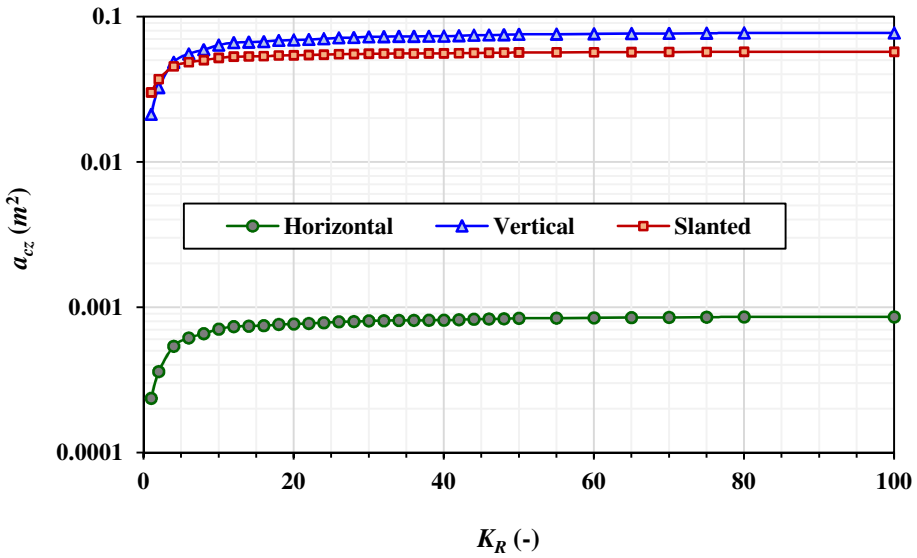

Fig. 7. Variations of the upgradient capture zone of NPRW (a_{cz}) versus relative hydraulic conductivity (K_R) for vertical well ($\hat{\theta} = 0$), slanted ($\hat{\theta} = 45^{\circ}$), and horizontal well ($\hat{\theta} = 90^{\circ}$) in a homogeneous and isotropic aquifer (Equation 16). In all cases well diameter D_w=0.03 m, and well length L_w=1 m.

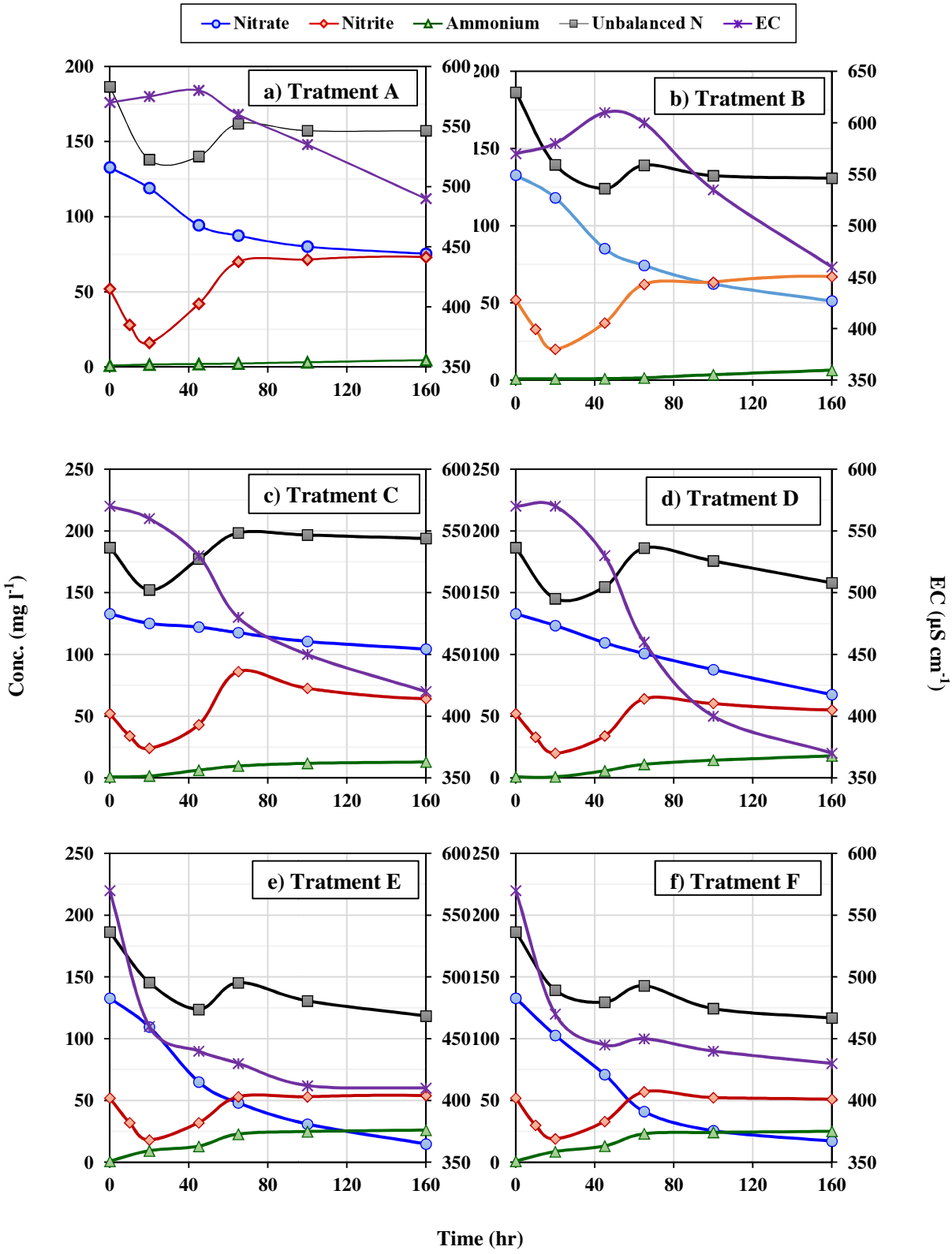

Fig. 8. Temporal variation of nitrate, nitrite, ammonium, total nitrogen, electrical conductivity (a to i) and pH (j) in batch experiments for nine treatments.

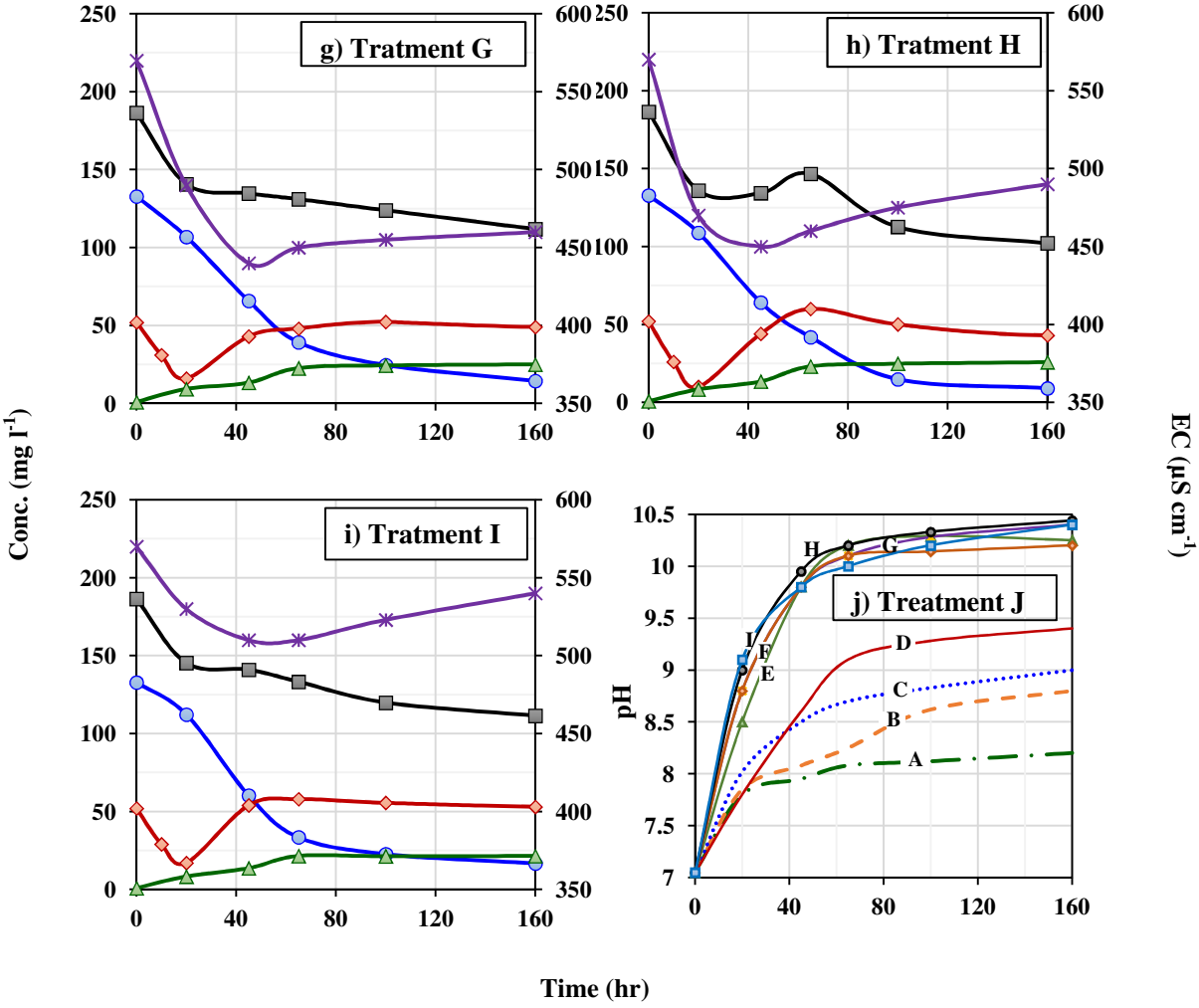

Fig. 8. Contineud.

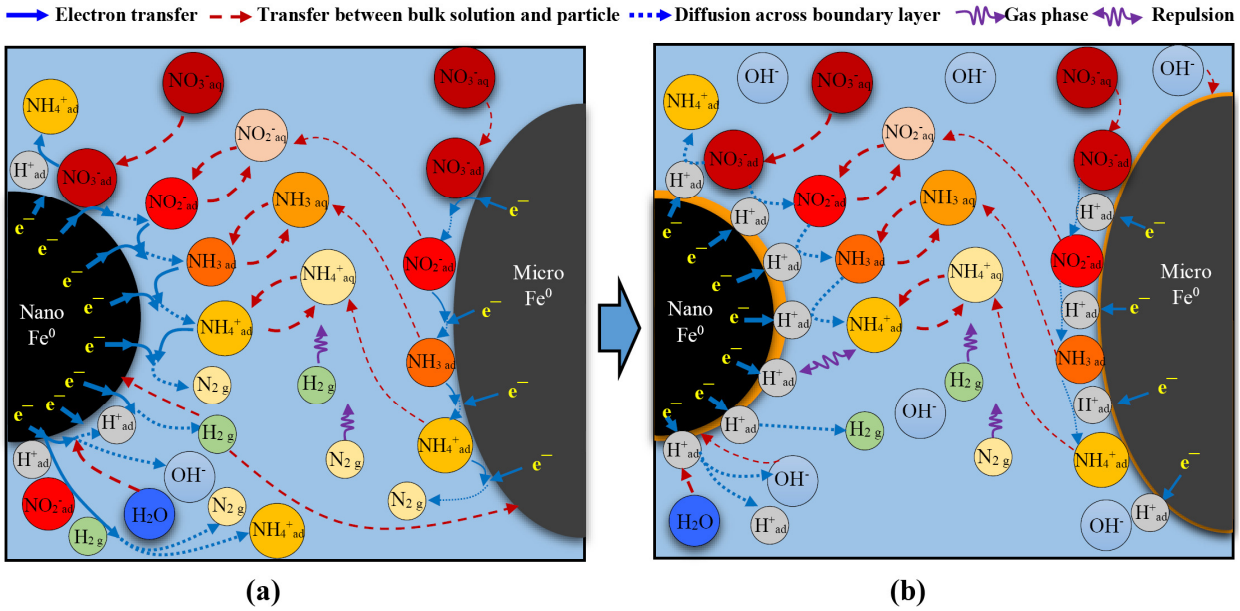

Fig. 9. Conceptual model of denitrification process by mixing NZVI and MZVI particles at early stage (a) and late stage of reaction (b).

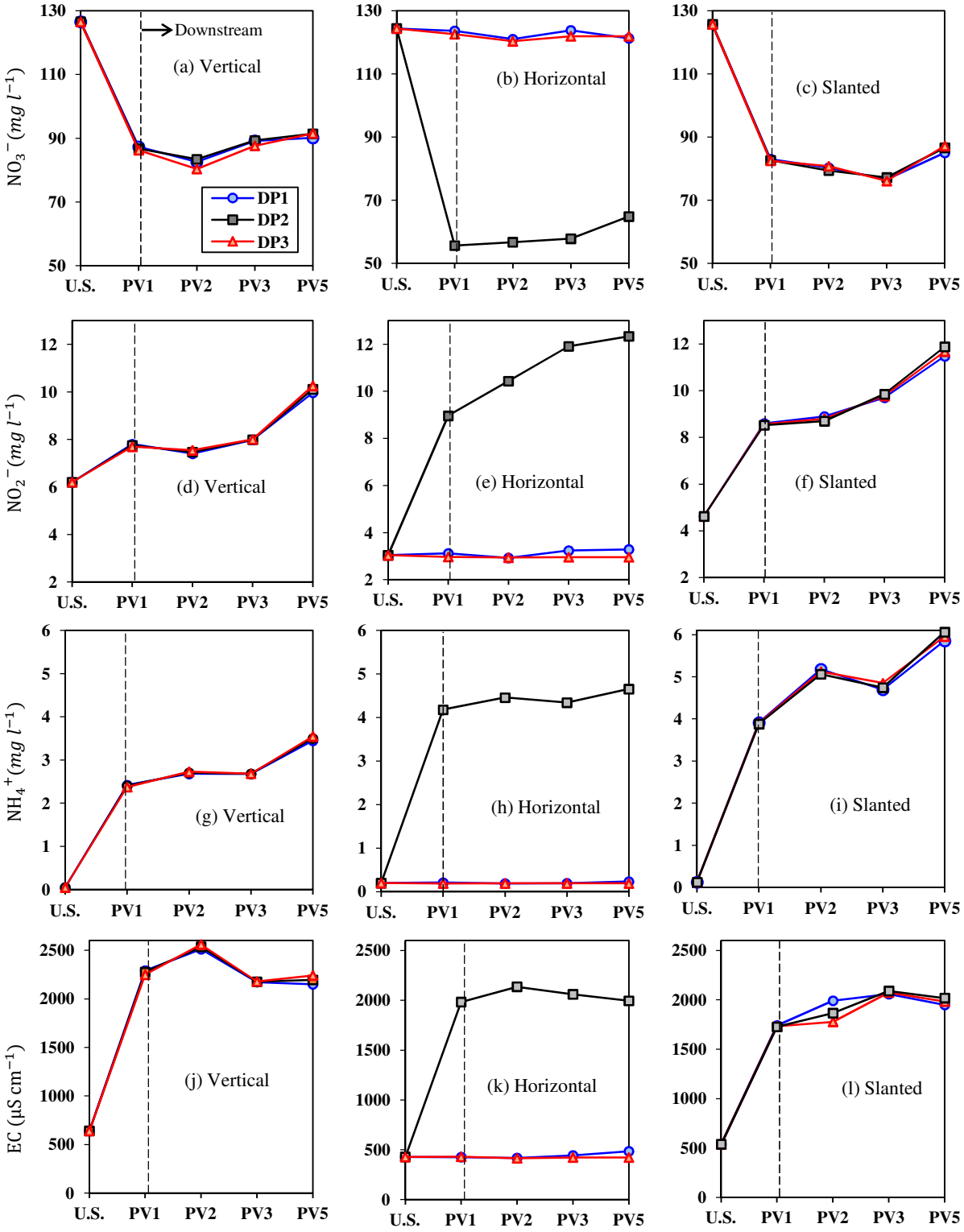

Fig. 10. Rate of Nitrate, nitrite, ammonium, electrical conductivity, and pH in groundwater effluent the NPRWs system at upstream piezometer (U.S.) and three downstream monitoring piezometers (DP1, DP2, and DP3) for different pore volumes (PV) and three orientations of NPRWs: vertical (a, d, g, j, and m), horizontal (b, e, h, k, and n), and slanted (c, f, I, d, and o). Vertical dashed line indicates the boundary between the values observed in upstream and downstream piezometers.

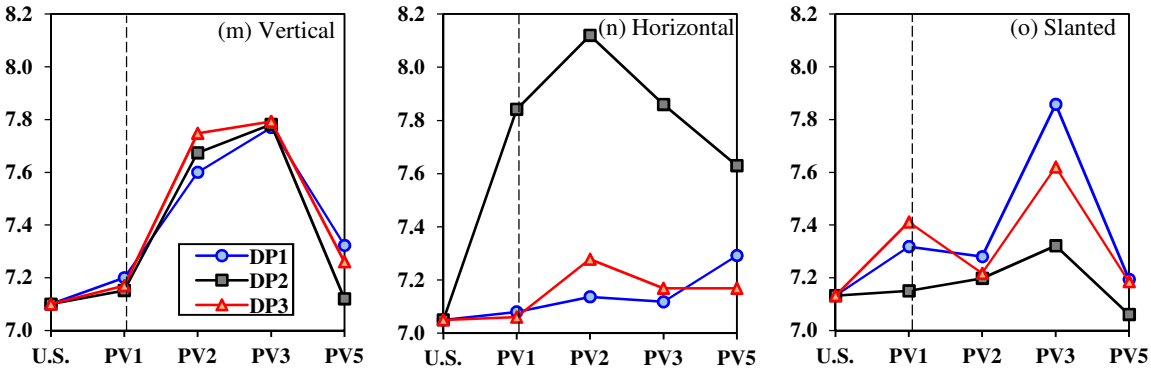

Fig. 10. Continued.

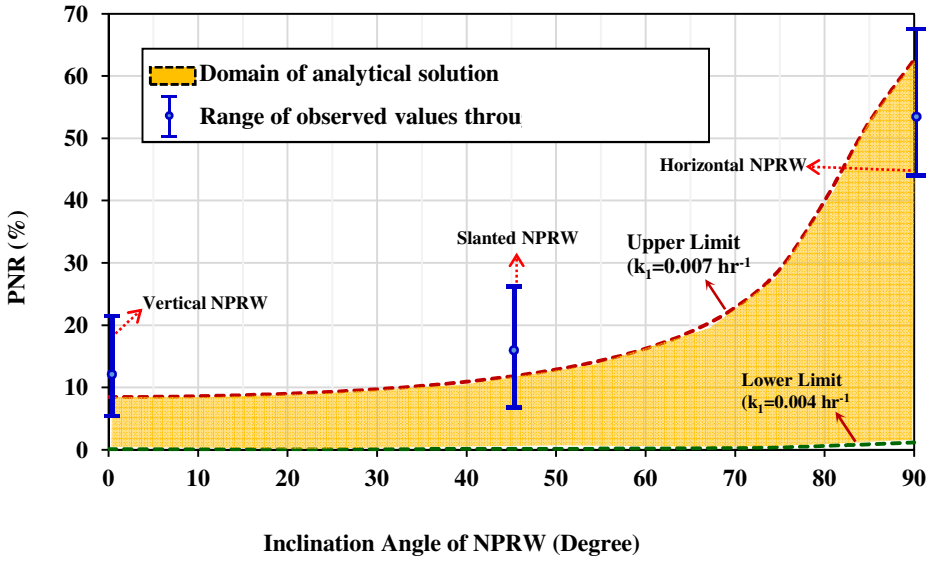

Fig. 11. Conformity between the percentages of Nitrate reduction (PNR) obtained by the analytical equations (equation 17) and those observed through the sand-box experiments. The upper and lower limits of analytical solutions are obtained based on sand-box experiment conditions, and also kinetic constants of Nitrate reduction (k_1) of the batch experiments.

8. Tables

Table 1. Concentration of reagents (NZVI and MZVI) used in the nine treatments. In each treatment, the weight ratio of reagents to containing initial mass of Nitrate are also given.

Reagent	**Treatment**								
	A	B	C	D	E	F	G	H	I
NZVI ($g\ l^{-1}$)	0.5	1.0	0.0	0.0	0.5	0.5	1.0	2.0	0.5
MZVI ($g\ l^{-1}$)	0.0	0.0	1.0	2.0	1.0	2.0	1.0	2.0	4.0
$NZVI/NO_3^-(g/g)$	3.75	7.5	0.0	0.0	3.75	3.75	7.5	15.0	3.75
$MZVI/NO_3^-(g/g)$	0.0	0.0	7.5	15.0	7.5	15.0	7.5	15.0	30.0
$Fe^0/NO_3^-(g/g)$	3.75	7.5	7.5	15.0	11.3	18.8	15.0	30.0	33.8

Table 2. Initial and final concentration of different species in solutions for batch tests (treatments A to I).

Species	**Initial**	**Long-Term Operation**								
		A	B	C	D	E	F	G	H	**I**
NO_3^- ($mg\ l^{-1}$)	133.0	4.9	5.2	12.5	7.5	2.5	6.0	6.7	2.5	**3.9**
NO_2^- ($mg\ l^{-1}$)	52.0	20.0	23.0	24.0	22.0	20.0	23.0	23.0	21.0	**21.0**
NH_4^+ ($mg\ l^{-1}$)	0.82	24.6	23.1	19.2	22.05	20.25	21.45	18.3	28.4	**25.6**
EC ($\mu S\ cm^{-1}$)	570.0	490.0	490.0	480.0	470.0	420.0	420.0	440.0	380.0	**390.0**
pH (-)	7.05	9.8	9.9	10.2	10.0	10.4	10.4	10.5	10.8	**10.6**

Table 3. Fitted kinetic constants of nitrate reduction rate (k_1), nitrite reduction rate (k_3), and stripping for two reaction stages (initial and late) for different treatments*.

Treatment	k_1 (h^{-1})		k_2(h^{-1})		k_3 (h^{-1})
	FRS	SRS	FRS	SRS	FRS
A	0.008 (0.980)	0.002 (0.939)	0.0060 (0.966)	0.0023 (0.937)	0.059 (0.999)
B	0.010 (0.960)	0.004 (0.985)	0.0106 (0.950)	0.0033 (0.973)	0.048 (0.999)
C	0.002 (0.911)	0.001 (0.971)	0.0081 (0.920)	0.0005 (0.971)	0.039 (0.996)
D	0.0042 (0.995)	0.0040(0.999)	0.0087 (0.990)	0.0009 (0.963)	0.048 (0.999)
E	0.015 (0.963)	0.012 (0.999)	0.0103 (0.977)	0.0012 (0.980)	0.053 (0.0997)
F	0.014 (0.998)	0.009 (0.962)	0.0104 (0.990)	0.0010 (0.999)	0.050 (0.995)
G	0.016 (0.977)	0.010 (0.988)	0.0117 (0.991)	0.0010 (0.995)	0.059 (0.999)
H	0.016 (0.964)	0.015 (0.928)	0.0169 (0.986)	0.0013 (0.990)	0.082 (0.991)
I	0.016 (0.935)	0.014 (0.876)	0.0111 (0.998)	0.0012 (0.926)	0.056 (0.999)

* Values in brackets show the R^2 values. FRS and SRS denote to first reaction step, and slow reaction step, respectively.